Exploring Synchrotron and Neutron Techniques for Characterizing Soft Knee Tissues

Bokvist Wrammerfors, Edvin Tobias

2026

Document Version:
Publisher's PDF, also known as Version of record

Exploring Synchrotron and Neutron Techniques for Characterizing Soft Knee Tissues

Edvin Tobias Bokvist Wrammerfors

LUND
UNIVERSITY

DOCTORAL DISSERTATION

by due permission of the Faculty of Engineering, Lund University, Sweden.
To be defended in Belfragesalen, BMC D15

Wednesday, June 10th, 2026 at 9.00

Public defence
June 10th, 2026, Belfragesalen
BMC D15, Lund University, Lund, Sweden

Supervisors
Prof. Hanna Isaksson
Department of Biomedical Engineering, Lund University, Lund, Sweden
Dr. Maria Pierantoni
Department of Biomedical Engineering, Lund University, Lund, Sweden
Prof. Martin Englund
Clinical Epidemiology Unit, Orthopedics, Department of Clinical Sciences Lund, Lund University, Lund, Sweden

Faculty opponent
Associate Professor Junning Chen
University of Exeter

Board of examination
Professor Luise Theil Kuhn
Technical University of Denmark, Copenhagen
Docent Alexandra Stubelius
Chalmers, Gothenburg
Dr. Robin Woracek
European Spallation Source, Lund
Docent Johan Hektor (suppleant)
Malmö University

Cover illustration: Front: neutron radiograph of two human articular cartilage samples acquired as part of a tomogram acquisition. Back: neutron radiograph of the same samples rotated 180 degrees.

Department of Biomedical Engineering
Lund University
P.O. Box 118, SE-221 00 Lund
Sweden
ISBN: 978-91-90202-27-2 (print)
ISBN: 978-91-90202-28-9 (electronic)
ISRN-nr: LUTEDX/TEEM-1152-SE
Report No. 3/26

Printed in May 2026 by Tryckeriet i E-huset, Lund, Sweden

Organization LUND UNIVERSITY	**Document name** DOCTORAL DISSERTATION
Department of Biomedical Engineering Box 118, 211 00 Lund, Sweden	**Date of issue** 2026-05-08
Author: Edvin Tobias Bokvist Wrammerfors	Sponsoring organization

Title: Exploring Synchrotron and Neutron Techniques for Characterizing Soft Knee Tissues

Abstract

Osteoarthritis (OA) is an age-related disease of the joint in which the tissues degenerate and the function of the joint is disrupted. Key load-bearing tissues that break down as part of knee osteoarthritis include the articular cartilage and the meniscus. These tissues are complex cartilaginous tissues, consisting of around 70% water confined in a network of collagens and proteoglycans. During OA, this network is disrupted by processes that are not yet fully understood resulting in inferior mechanical properties of the tissues and eventually pain and loss of mobility for the patient.

Traditionally pathologies of cartilaginous tissues are studied via magnetic resonance imaging (MRI)-based techniques as well as histological slicing and staining, which carry several limitations. MRI is a powerful technique that is usable both in vivo and on ex vivo samples but is limited in resolution and often produces complex signals that can be difficult to interpret. Histology provides excellent characterization of cell features and matrix composition but is limited to 2D and requires ex vivo samples, fixation and slicing, which alters the state of the tissue and consequently limits sequential experiments.

Several novel approaches seeking to address these limitations exist, the work in this thesis being focused on examining whether new insights into tissue properties and the degeneration process can be gained by three main techniques: synchrotron phase-contrast tomography, neutron tomography, and quasi-elastic neutron scattering (QENS) for the examination of ex vivo samples. More specifically, the aim was to study in 3D distribution of cells, protein matrix density, and water diffusivity within tissues as well as potential changes induced by OA-related degeneration.

Phase-contrast in X-rays circumvents many of the limitations with applying X-rays to the study of soft tissue by producing contrast not only from absorption but also from transitions between materials. The addition of the powerful beams produced by synchrotron sources enables rapid, high-volume measurements while preserving the tissue in a close to native state.

Neutrons can be used for tomography in a similar manner to X-rays, but interact strongly with certain light elements, particularly hydrogen. Additionally, they are sensitive to isotopes, which allows heavy water to be used as a contrast agent. Furthermore, the low energies of neutrons allow small changes in energy to be detected, which enables the study of water or other molecular dynamics via QENS.

The first study employs synchrotron phase-contrast tomography to examine human articular cartilage samples. Samples from both donors and total knee replacement patients were imaged and chondrocytes segmented. Results show several degeneration features in similar or better quality than histology as well as depth-dependent associations between cell properties and degeneration level. The second and third studies employ neutron tomography to study protein density and water diffusion in cartilage and meniscus. Human articular cartilage samples were imaged in an exploratory study, showing the best contrast in heavy water-treated samples as well as revealing clear differences in depth-dependent protein matrix density depending on disease state. Then in the third study, bovine cartilage and meniscus samples were imaged during the exchange of water and heavy water, showing long-range macroscopic diffusion in the tissue. The fourth study employed QENS to directly probe water dynamics in bovine articular cartilage. Samples from different depths were measured, producing a measure of fast water dynamics and slower molecular movements at the nanosecond scale. Results show that the restriction of water diffusion within the cartilage is more complex than a simple reduction of diffusion speeds at short enough length scales.

In summary, the work presented in this thesis shows the potential of synchrotron and neutron techniques for the study of ex vivo cartilaginous tissues. Initial experiments have provided a baseline for what these techniques reveal, showing the potential for future experiments, such as altered water dynamics with loading or degeneration, or novel ways of categorizing cartilage degeneration based on phase-contrast volume imaging.

Key words: Articular cartilage, meniscus, knee OA, neutron imaging, synchrotron imaging, QENS, water dynamics

Classification system and/or index terms (if any)

Supplementary bibliographical information ISRN: LUTEDX/TEEM-1152-SE Report No. 3/26		**Language:** English
		ISBN: 978-91-90202-27-2 (print) ISBN: 978-91-90202-28-9 (electronic)
Recipient's notes	**Number of pages: 180**	Price
	Security classification	

Populärvetenskaplig sammanfattning

En av de vanligaste anledningarna till minskad rörlighet med ålder är artros, en ledsjukdom som påverkar över en fjärdedel av den svenska befolkningen över 45 år. Artros orsakas av långsam nedbrytning av ledernas vävnader, vilket i sin tur kan leda till stelhet och smärta i leden. I dagsläget finns inga behandlingar som kan stoppa själva nedbrytningen, så sjukdomen behandlas i princip bara med rörelse, smärtstillande, och i långt gångna fall med operation med ledprotes. Den leden som oftast drabbas av symptomgivande artros är knäet.

Knäleden består av tre ben (lårben, smalben, och knäskål) som i ändarna är täckta av ledbrosk. Mellan lårbenet och smalbenet sitter meniskerna, två broskliknande halvmåneformade ”kilar” med stötdämpande och stabiliserande funktion. Leden hålls ihop av ett antal ligament och omges av en hinna som inrymmer ledvätska. Meniskerna och ledbrosket består till ~70% av vatten, och till resten av proteinnätverk. Dessa proteinnätverk består främst av kollagenfibrer som bildar en matris som håller samman vävnaden. Utspridd i denna matris finns proteoglykaner som drar till sig vatten och därigenom ger upphov till vävnadens unika mekaniska egenskaper. Vid artros så förstörs organisationen av dessa proteinnätverk successivt, vilket ändrar vävnadens mekaniska egenskaper vilket i slutändan leder till förlust av vävnad och smärta vid rörelse. Grundorsakerna till artros saknar idag fullständig förståelse, vilket försvårar försök att utveckla behandlingar. Därför behövs nya tekniker för att studera förändringar i dessa vävnader.

I denna avhandling utforskas tre nya tekniker på brosk: faskontrast-synkrotrontomografi, neutrontomografi, och kvasi-elastisk neutronspridning. Samtliga dessa tekniker kräver storskaliga faciliteter (synkrotroner eller neutronkällor) av den sort som nyligen har byggts i Lund i form av MAX IV och ESS. Det tidigare användningsområdet av dessa tekniker på brosk är ytterst

begränsat eller helt obefintligt och därför finns stort nyhetsvärde i att utforska dess möjligheter att studera egenskaper såsom cellfördelning, proteintäthet, eller vattenrörelser i vävnaden.

Tomografi, även känt som datortomografi och vanligtvis förkortat till CT (för ”computed tomography”), är en teknik som skapar tredimensionella bilder med hjälp av genomlysning, oftast av röntgen. Ett antal genomlysningsbilder (t.ex. vanliga röntgenbilder) tas medan det som ska avbildas roteras. Från dessa tvådimensionella bilder kan sedan en tredimensionell bild räknas ut. Faskontrastsynkrotrontomografi gör denna teknik kraftfullare på två sätt. För det första så används en synkrotron, en slags partikelaccelerator som producerar extremt kraftig koherent röntgenstrålning. Denna kraftiga stråle tillåter mycket snabbare och mer högupplöst avbildning än en röntgenkälla i ett labb eller sjukhus. För det andra så kompletteras den sedvanliga kontrasten i röntgenbilder (absorptionskontrast, som kommer från att röntgenstrålar blockeras) med kontrast från fasskifte i koherenta röntgenstrålar. Ett fasskifte uppstår när röntgenstrålningen passerar från ett material till ett annat, till exempel från broskvävnad till en broskcell. När strålningen är koherent, det vill säga att hela strålen har samma fas från början, så kan detta fasskifte avbildas som en kontrast som uppstår på grund av interferens vid längre propagationsavstånd för strålarna. Denna faskontrast är mycket starkare än absorptionskontrast i lätta, mjuka material som släpper igenom majoriteten av röntgenstrålningen.

Neutrontomografi fungerar på samma principer, men använder neutroner i stället för röntgenstrålning. Neutroner är oladdade partiklar vars interaktion med material främst påverkas av hur atomkärnan är uppbyggt. Neutrontekniker är därför känsliga för vissa lätta material som syns dåligt med röntgen, speciellt väte. Dessutom är neutroner känsliga för isotoper, vilket innebär att man kan använda deuterium (tungt väte, en väteatom med en extra neutron) som ett kontrastmedel. I biologiska material ger neutrontomografi därför en bild av hur väte är fördelat i materialet, och tillåter en att skilja på ”löst” väte (som det i vatten) och det som är bundet i proteiner eller andra delar av vävnaden genom att byta ut det lösa vätet mot deuterium. En annan egenskap är att neutronstrålning har relativt låg energi i de individuella neutronerna jämfört med t.ex. röntgenstrålning. Denna energi är nära energin som finns i molekylära rörelser, såsom i vattenmolekyler som diffunderar. Genom att mäta hur mycket neutronernas energi ändras när de sprids i material med rörliga molekyler kan man därför studera molekylrörelserna i materialet med en teknik som kallas kvasi-elastisk neutronspridning.

I den första studien i avhandlingen studeras mänskliga broskprover med olika grader av nedbrytning med faskontrastsynkrotrontomografi. Tekniken används för att avbilda cellerna inuti brosket samt olika fiberstrukturer vid broskets yta som förändras vid nedbrytning. Detta resulterade i bilder med jämförbar kvalitet till klassisk histologi (färgade mikroskopibilder), men tillät avbildning i tre dimensioner samt i ett mer naturligt tillstånd än i mikroskopi, vilket ger en bättre helhetsbild av

vävnadens egenskaper. Cellernas form och fördelning i brosket kunde även undersökas, vilket visade på samband mellan vissa cellulära egenskaper och graden av nedbrytning i brosket.

I den andra och tredje studien i avhandlingen studeras brosk med neutrontomografi. Först studeras mänskligt brosk för att undersöka samband mellan vätetäthet i vävnaden och sjukdomstillstånd. Det visade sig att vätetätheten varierar mer med ökad nedbrytning av brosket. Detta följdes sen upp med en studie på vattendiffusion i brosk och menisk. Här avbildas vävnaderna med neutroner kontinuerligt samtidigt som tungt vatten diffunderar in i vävnaden. Detta ger en bild av ändringarna i vattenhalt över tid, vilket i sin tur kan komplettera MR-baserade mätningar av diffusionshastighet.

I den fjärde studien i avhandlingen studeras tunna skivor av brosk med kvasi-elastisk neutronspridning. Brosket delades upp baserat på dessa djup, och sedan studerades både snabbare rörelser såsom vattendiffusion, samt långsammare rörelser såsom förflyttningar av proteiner. Både studie 3 och 4 ger en grundläggande förståelse för hur vattendynamiken ser ut i frisk, obelastad vävnad, vilket kan användas som grund för framtida forskning kring förändringar med sjukdomsstadium eller mekanisk belastning.

Sammanfattningsvis så utforskar avhandlingen nya avancerade tekniker av den typ som finns tillgängliga på MAX IV och inom snar framtid ESS för att studera brosk. Den visar potentialen och begränsningar med dessa tekniker, vilket förhoppningsvis kan utgöra grunden för framtida forskning som utröner hur brosk och meniskvävnader får sina unika egenskaper, samt hur och varför de långsamt bryts ner vid artros.

Abstract

Osteoarthritis (OA) is an age-related disease of the joint in which the tissues degenerate and the function of the joint is disrupted. Key load-bearing tissues that break down as part of knee osteoarthritis include the articular cartilage and the meniscus. These tissues are complex cartilaginous tissues, consisting of around 70% water confined in a network of collagens and proteoglycans. During OA, this network is disrupted by processes that are not yet fully understood resulting in inferior mechanical properties of the tissues and eventually pain and loss of mobility for the patient.

Traditionally the pathologies of cartilaginous tissues are studied via magnetic resonance imaging (MRI)-based techniques as well as histological slicing and staining, which carry several limitations. MRI is a powerful technique that is usable both in vivo and on ex vivo samples but is limited in resolution and often produces complex signals that can be difficult to interpret. Histology provides excellent characterization of cell features and matrix composition but is limited to 2D and requires ex vivo samples, fixation and slicing, which alters the state of the tissue and consequently limits sequential experiments.

Several novel approaches seeking to address these limitations exist, the work in this thesis being focused on examining whether new insights into tissue properties and the degeneration process can be gained by three main techniques: synchrotron phase-contrast tomography, neutron tomography, and quasi-elastic neutron scattering (QENS) for the examination of *ex vivo* samples. More specifically, the aim was to study in 3D distribution of cells, protein matrix density, and water diffusivity within tissues as well as potential changes induced by OA-related degeneration.

Phase-contrast in X-rays circumvents many of the limitations with applying X-rays to the study of soft tissue by producing contrast not only from absorption but also from transitions between materials. The addition of the powerful beams produced

by synchrotron sources enables rapid, high-volume measurements while preserving the tissue in a close to native state.

Neutrons can be used for tomography in a similar manner to X-rays, but interact strongly with certain light elements, particularly hydrogen. Additionally, they are sensitive to isotopes, which allows heavy water to be used as a contrast agent. Furthermore, the low energies of neutrons allow small changes in energy to be detected, which enables the study of water or other molecular dynamics via QENS.

The first study employs synchrotron phase-contrast tomography to examine human articular cartilage samples. Samples from both donors and total knee replacement patients were imaged and chondrocytes segmented. Results show several degeneration features in similar or better quality than histology as well as depth-dependent associations between cell properties and degeneration level.

The second and third studies employ neutron tomography to study protein density and water diffusion in cartilage and meniscus. Human articular cartilage samples were imaged in an exploratory study, showing the best contrast in heavy water-treated samples as well as revealing clear differences in depth-dependent protein matrix density depending on disease state. Then in the third study, bovine cartilage and meniscus samples were imaged during the exchange of water and heavy water, showing long-range macroscopic diffusion in the tissue.

The fourth study employed QENS to directly probe water dynamics in bovine articular cartilage. Samples from different depths were measured, producing a measure of fast water dynamics and slower molecular movements at the nanosecond scale. Results show that the restriction of water diffusion within the cartilage is more complex than a simple reduction of diffusion speeds at short enough length scales.

In summary, the work presented in this thesis shows the potential of synchrotron and neutron techniques for the study of *ex vivo* cartilaginous tissues. Initial experiments have provided a baseline for what these techniques reveal, showing the potential for future experiments, such as altered water dynamics with loading or degeneration, or novel ways of categorizing cartilage degeneration based on phase-contrast volume imaging.

List of appended papers

I. **B. Wrammerfors ET**, Pierantoni M, Dejea H, Sjögren A, Orozco G, Das Gupta S, Gstöhl S, Schlepütz C, Nygård K, Englund M, Isaksson H. *Synchrotron phase-contrast microtomography reveals the impact of degeneration on the 3d structure of human articular cartilage.* Osteoarthritis and Cartilage. 2026. doi: 10.1016/j.joca.2026.04.001

The study was designed by the supervisors. Sample preparation and microtomography experiments were performed by multiple co-authors with ET B. Wrammerfors performing some of them. ET B. Wrammerfors was responsible for conducting data analysis and interpretation for all experiments. Histology and scoring were performed by other co-authors, but quantification of histology was performed by ET B. Wrammerfors. ET B. Wrammerfors was responsible for writing the manuscript.

II. **B. Wrammerfors ET**, Törnquist E, Pierantoni M, Sjögren A, Tengattini A, Kaestner A, in 't Zandt R, Englund M, Isaksson H. *Exploratory neutron tomography of articular cartilage.* Osteoarthritis and Cartilage. **2024**;32(6):702-12. doi: 10.1016/j.joca.2024.02.889

The study was designed by the supervisors with substantial contributions from ET B. Wrammerfors. ET B. Wrammerfors was responsible for preparing samples and carrying out experiments with support of co-authors. ET B. Wrammerfors was responsible for data analysis and interpretation of data from all experiments. Histology and scoring were performed by other co-authors. ET B. Wrammerfors was responsible for writing the manuscript.

III. **B. Wrammerfors ET**, Jönsson V, Sharma K, Tengattini A, Or K, Topgaard D, Isaksson H, Pierantoni M. *Neutron imaging to quantify diffusion in knee joint tissues*. Manuscript under review. 2026.

ET B. Wrammerfors was largely responsible for the design of this study together with the supervisors. ET B. Wrammerfors was responsible for sample preparation, beamtime application, and neutron imaging experiments. Diffusion tensor imaging experiments were performed jointly with co-authors. ET B. Wrammerfors was responsible for analysis and interpretation of neutron data, Diffusion tensor data was analysed and interpreted jointly with co-authors. The computational modelling was performed by co-authors and interpreted jointly. ET B. Wrammerfors was responsible for writing the manuscript.

IV. **B. Wrammerfors ET**, M. Björklund N, Seydel T, Sjögren A, Englund M, Pierantoni M, Isaksson H. *Investigating water dynamics in knee articular cartilage via QENS*. Manuscript. 2026.

ET B. Wrammerfors was largely responsible for the design of this study. ET B. Wrammerfors was responsible for sample preparation, beamtime application, and QENS experiments. Each part was supported by co-authors. ET B. Wrammerfors was largely responsible for data analysis and interpretation. ET B. Wrammerfors was responsible for writing the manuscript.

Acknowledgements

As I enter the final hours of work on the version of this thesis that you are likely now holding in your hands I face a challenge of a different nature yet maybe just as difficult as wrapping one's mind around the many intricacies of neutrons. How, exactly, does one do justice to everyone who ought to be acknowledged while still writing a statement short enough that people will actually read it? As to whether I have found an answer, well, we will see if you are still reading at the end.

First, I would like to thank Hanna, who took a chance on someone who was not in a great place when this journey started in early 2021, and who has given me far more grace than I deserve when the time needed for it grew a bit longer than it should have been. I would also like to thank Maria, for likewise being patient with me when I was a bit to stubborn in the face of what was always very good feedback, for making sure no detail was neglected, and for guiding me through the everyday practicalities of doing research. Finally, I would like to thank Martin for giving me insight into the medical side of things, letting me peer outside my engineering bubble to see how vast this field can be.

Next my colleagues past and present, whom I have many more things to thank for than I will manage to list here. Elin, who brought me to my first beamtime and whipped me into shape when I grumbled a tad to much. Thomas and Joeri, only one of whom I managed to trick into drinking besk. Isabella, who gave much needed words of encouragement when I felt I was getting less done than I should. Gustavo, who I still think should have gotten a Finnish PhD sword. Hector, who led me to enjoy the synchrotron (almost) as much as the neutron source. Kunal, who has been here since the start, probably deserved this project more than me, and who has been a constant voice of encouragement. Chiara, Lauren, and Julio, who made sure we always had a jovial atmosphere in the office. Lorenzo, Yeswanth and Shuvashis, who always made sure I get my coffee breaks. Viktor, who both let me glimpse the computational world and who makes great kladdkaka. Lea, who has always been one

step ahead of me since long before either of us started our PhDs. Shoaib, who I almost managed to pull into the Lundensian student sphere. Jenny, Anna, and Worapat, who always brought a good mood to lunch and coffee. Sana, who happily listened to me ramble about food for way too long. Noa, who brought an insatiable curiosty to everything we were doing. And then, of course, everyone elso who has been through the group while I was here; there are too many of you to list, but all of you have made my journey brighter in large or small ways.

Then there are all the others that I worked with. Amanda, who put up with my million questions about histology, and guided me through a decidedly nonstandard means of slicing cartilage. Christian and Kim, who showed me the way around two different synchrotrons. Alessandro, Anders, and Tilo, who taught me about neutrons from many different angles. René, Kenneth, and Daniel, who helped me understand MRI as something other than black magic. Then of course both all of SwedNESS and all the ILL PhD students, who introduced me to two different wonderful neutron communities.

And here, dear reader, you may think I was winding down, but I am only halfway through. It seems that the answer to the question I opened with may yet elude me, as I move into all the support I have gotten outside of the confines of the lab.

First I would like to thank my family, for far more things than the few I am able to mention here. My mom and dad, who nurtured my interest in science for longer than I can remember, who supported me without question when I wanted to move halfway across the world to get back to Sweden for my studies, and who have always provided the security that is far too easy to take for granted. Pelle, who I know I could always turn to for support, which helped even if I rarely found the right words to do so. Maja, who I quite possibly bewildered with a quite sudden tour of MAX IV when she visited. And Erik, who of all my siblings quite possibly most reminds me of myself; might they be writing something much like this in ten years' time?

Next I want to thank my friends both old and new. First, there is Valkyrie, who has always been the first to listen to me when things go wrong. Who has been the source of endless discussions on essentially every topic that can be imagined, who humors me when I think up ancient elves with necromantic synchrotrons for my games, and who even occasionally grants me access to her boundless wit to shower me in neutron jokes. (Or to threaten to replace all my neutrons with snails.) Then there is the rest of the Hydra, who have all been there for me in many ways. Christina, with whom I have all too many times driven Valkyrie to boredom by discussing all the intricacies of academia. Jack, who of all my high school friends has put the most energy into staying in touch. Pelle, who I have already mentioned, but who bridges the gap between family and friends. Then of course Nick, Holly, Will, Eric, and Ben, D&D-players old and new.

While at the start of my journey I may have thought old friends were enough, I am very glad that that is not the case. I would like to thank Alex and Franzi for leading me back into the student sphere via Dokt, rekindling old joy that I had thought lost at a time when I was thoroughly stuck in the post-pandemic blues. I would like to thank both dokt itself and all my fellow Dokt board members both my year and the next, for setting me on the path to actually rebuild my social life. Especially I would like to thank Oscar, who succeeded me as project coordinator, and Simon, who was instrumental into helping me become properly social again.

Then I would like to thank Kalmar Nation and all the people who I met there, for letting me rediscover student life in the last few years I spend as a student. Hadiqa for letting me know the Kalmar discord existed, without which I may never have found my way back there. Fragancia and Mika for the well-timed civ game, goat burning, and book club that led me to actually return in person. Simon again for making sure I actually returned to the pub. Love, Broman, Hugo, and Jose for getting me properly involved and making sure I stuck around. Heyner and Zeynep for being familiar faces that let me not feel too out of place. Alice for being a fantastic fellow editor of the paper, and bringing the artistic skill I sorely lack. And of course, many more, everyone I have spoken to in the pub who helped me feel welcome, every worker I confused with odd requests, everyone who let me design a silly drink in their name, everyone whose ear I have talked off, everyone who I pestered to go read Valkyrie's writing, all my fellow foremen. I would list you all, but I fear I have already lost most readers of this section.

Finally I would like to thank all of those I have forgotten. As I write this, I have hours at most to spare before all of this needs to be sent to print, so chances are low that someone has slipped my mind. So, just because I did not mention you does not mean I am not thankful, just that I am quite fallible.

And at last I would like to thank you, dear reader who has actually read this through to the end rather than skipping ahead or scanning for your name. I do not think I have kept this short enough for you to deserve any less, for while many questions are answered within these pages, how to keep an acknowledgement short enough for all to read is not among them.

Tobias Wrammerfors

Lund, May 2026

List of abbreviations

2D	two-dimensional
3D	three-dimensional
CT	computed tomography
DESY	Deutsches Elektronen-Synchrotron
DTI	diffusion-tensor imaging
ESRF	European Synchrotron Radiation Facility
ESS	European Spallation Source
FOV	field of view
H&E	hematoxylin and eosin
ILL	Institute Laue-Langevin
J-PARC	Japan Proton Accelerator Comples
MRI	magnetic resonance imaging
NMR	nuclear magnetic resonance
OA	osteoarthritis
OARSI	Osteoarthritis Research Society International; OA grading Standard
PBS	Phosphate-buffered saline
PFTE	Polytetraflouroethylene
PSI	Paul Scherrer Institut

QENS	quasi-elastic neutron scattering
NT	neutron (micro)tomography
Saf-O	Safranin-O and Fast Green
SLS	Swiss Light Source
SINQ	Swiss Spallation Neutron Source
SNS	Spallation Neutron Source
VOI	volume of interest
XRT	x-ray (micro)tomography

Table of Contents

1 Introduction

One of the major leading causes of age-related disability is osteoarthritis (OA), with over 600 million people affected worldwide, including more than a quarter of the Swedish population above age 45 (1-3). This disease involves degeneration of the load-bearing soft tissues of the joints, with the knee joint being the most commonly affected. Degeneration affects all parts of the joint, but most prominently the articular cartilage and meniscus, and has an array of complex causes that are not fully understood (1, 4).

Clinically, knee OA primarily presents as pain in the joint, either when moving or chronically. Stiffness which further restricts motion is also common, especially in the morning (1, 4). The limited mobility imposed by these symptoms leads to physical disability, impeding both patient quality of life and ability to work as well as increasing the risk of comorbidities such as cardiovascular diseases (4). Diagnosis is determined from these symptoms, in conjunction with clinical imaging when needed. If so, X-ray radiographs, X-ray CT (computed tomography), or magnetic resonance imaging (MRI) may play an important role to determine the extent of the degeneration of the joint or to exclude other diagnoses than OA(1, 4).

Pre-clinically, degenerative changes in joint tissues are primarily studied via histological, MRI, and CT-based techniques, which come with a number of limitations. Histology is currently the gold standard for detailed *ex vivo* OA evaluation (5), but suffers from the hard requirement of fixation as well as cutting the tissue into slices. Thus, it provides only 2D information. MRI offers a number of powerful techniques for measuring biochemical composition of cartilage, albeit in a complex manner which results in correlations that are challenging to interpret (6). Moreover, although MRI provides 3D information, it has limited resolution.

Consequently, there are potential benefits with exploring novel techniques for characterizing knee joint tissues. Cartilage is a soft tissue with a high water content, with the dry component primarily consisting of collagen and proteoglycans

interspersed with chondrocyte cells (7). Phase-contrast X-rays allow for probing of cells and fibrillations by revealing transitions between different tissue phases, while neutron techniques allow one to probe the hydrogen-, and consequently water content and dynamics of the tissue.

X-ray tomography (XRT) using phase-contrast enhancement has shown substantial promise in acquiring images of soft tissues with histology-like fidelity in full 3D (8), especially when making use of the powerful beams available at synchrotron sources. This technique has been applied to the study of meniscus with great promise (9), but applications to cartilage has this far been limited to smaller sample sets (10, 11) despite the high throughput of synchrotron imaging allowing for large sets to be rapidly imaged.

Another technique which is almost entirely unexplored in the field of soft tissue studies is neutron tomography (NT). NT functions on similar principles as XRT, but with neutrons rather than X-rays, resulting in different sources of beam attenuation. In biological tissues, the primary source of neutron attenuation is hydrogen, resulting in NT essentially producing a map of hydrogen density (12). Additionally, neutrons are sensitive to isotopes which allows for the use of heavy water (D_2O) as a contrast agent with a factor seven lower attenuation than regular water (13). This has previously been used as a general proof-of-concept in biology (12), to study hydration and water movement in plant tissues (14-16) and in bone (17, 18), but remains unexplored in soft musculoskeletal tissues.

Furthermore, neutrons can be used to study water and protein dynamics directly via quasi-elastic neutron scattering (QENS) (19, 20). QENS functions by measuring the small energy shifts (μeV-meV range) in neutrons caused by scattering off of a moving molecule. In biological tissues, the primary scatterer is hydrogen, resulting in water being the primary component measured. This has previously been applied both to idealized protein solutions (21), whole tissues (22), and to changes in dynamics caused by mechanical stress (23). With articular cartilage being a complex tissue dependent on water dynamics for its load-bearing ability, QENS is of natural interest for deepening knowledge of its dynamics.

Access to both neutron and synchrotron techniques has recently been substantially expanded in Sweden with the construction of the MAX IV synchrotron (24) and the European Spallation Source (ESS) (25) in Lund, Sweden. At MAX IV, multiple beamlines such as ForMAX (26) or DANMAX (27) offer phase-contrast imaging capabilities alongside other material characterization techniques. Once ESS opens for user operation in 2027, high-performance neutron imaging will be offered at the ODIN beamline (28), and a number of spectroscopy beamlines such as CSPEC and MIRACLES (25) will be able to perform QENS measurements.

This work explores the application of the described techniques to soft knee tissues, primarily to articular cartilage and to some extent to the meniscus. A large cohort of

human articular cartilage samples were imaged with phase-contrast X-ray tomography, with a subset also being imaged with neutron tomography. Neutron tomography was then applied to study water dynamics in the form of macroscale water diffusion in bovine articular cartilage and meniscus, and QENS was applied to directly study cartilage water dynamics.

2 Aim and design of the thesis

The overall aim of this thesis work was to investigate novel applications of synchrotron and neutron techniques to the study of soft knee joint tissues, particularly the articular cartilage. This work identifies and explores applications of these techniques to cartilage and meniscus characterization with the goal of evaluating which information can be gained and applied to the study of osteoarthritic degeneration and tissue water diffusivity, paving the way for expanded future usage.

The aims of the individual studies were:

I. To investigate synchrotron phase-contrast imaging on a large dataset of human cartilage with the goal of determining the qualitative and quantitative effects of tissue degeneration on cell and tissue matrix properties.

II. To explore neutron imaging of human articular cartilage, determining the best preparation methods for imaging as well as to what extent degeneration affect the tissue protein density distribution.

III. To apply neutron tomography to study water dynamics in bovine articular cartilage and meniscus in the form of D_2O-H_2O exchange, with the goal of quantifying macroscopic diffusion.

IV. To probe water dynamics in bovine articular cartilage with quasi-elastic neutron scattering, discerning diffusion modalities and evaluating the ability to distinguish depth-dependent dynamics.

The design of the thesis is outlined in Figure 2.1.

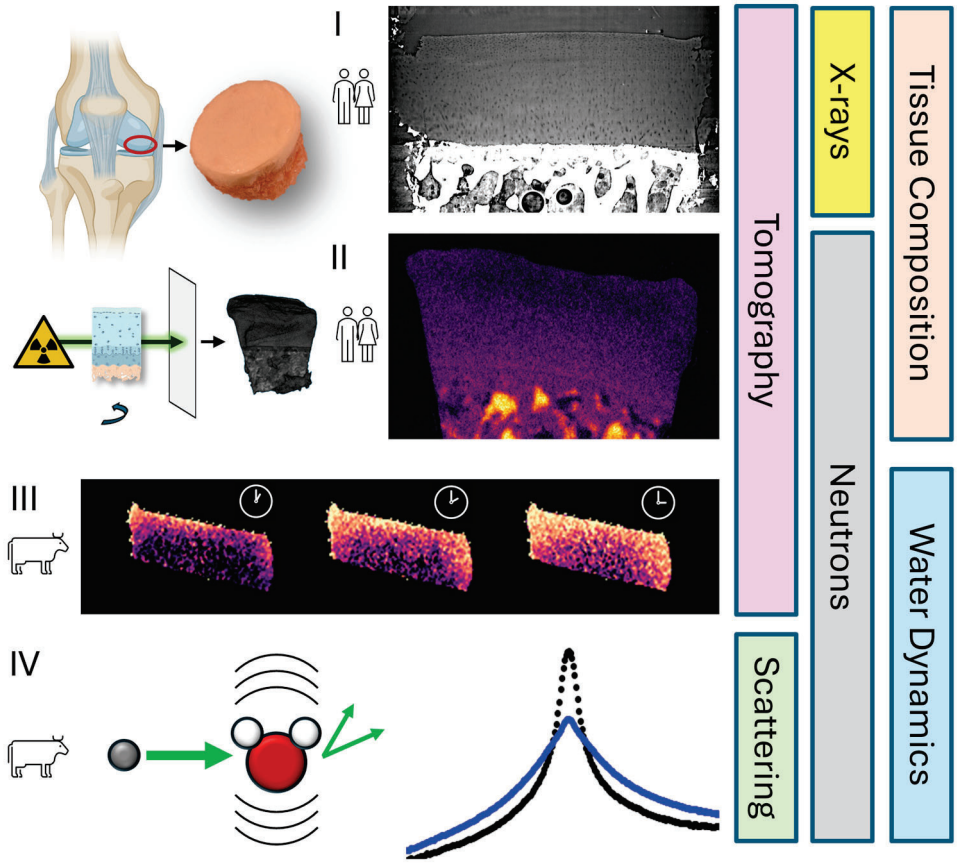

Figure 2.1: Graphical abstract. Top left: Sampling location and example cartilage plug as well as schematic depiction of tomography. The roman numerals (I-IV) indicate the studies included in the thesis. The icons indicate from where tissue samples were obtained (human or bovine). Studies are categorized by technique and object of study on the right.

3 Background

In this section the structure of articular cartilage and meniscus are described, including how they are affected during osteoarthritis. This is followed by explanations of the various techniques used to characterize the tissues within this work.

3.1 Knee Joint Tissues

The knee joint is one of the largest joints in the body, connecting three major bones (the femur, tibia, and patella). The ends of the bones are covered in articular cartilage, providing both a low-friction articulating surface as well as shock-absorbing properties (7) (Figure 3.1a). Dividing the joint into a medial and lateral compartment is the central pivot, secured by the anterior and posterior cruciate ligaments (29). Within each compartment is a meniscus, which serves to distribute load and stabilize the joint by acting as a mobile cushion of cartiliginous tissue (29, 30) (Figure 3.1b). Further support for the joint is provided by the collateral ligaments as well as the encasing fibrous joint capsule containing the synovium (31).

As one of the primary joints supporting the weight of the human body during walking or other regular motion, the knee has to sustain substantial continuous loads. Much of this load is carried by the articular cartilage and mensicus. Consequently, understanding the function of these tissues is of substantial

importance for understanding both the healthy knee and the progression of OA (1, 30, 32).

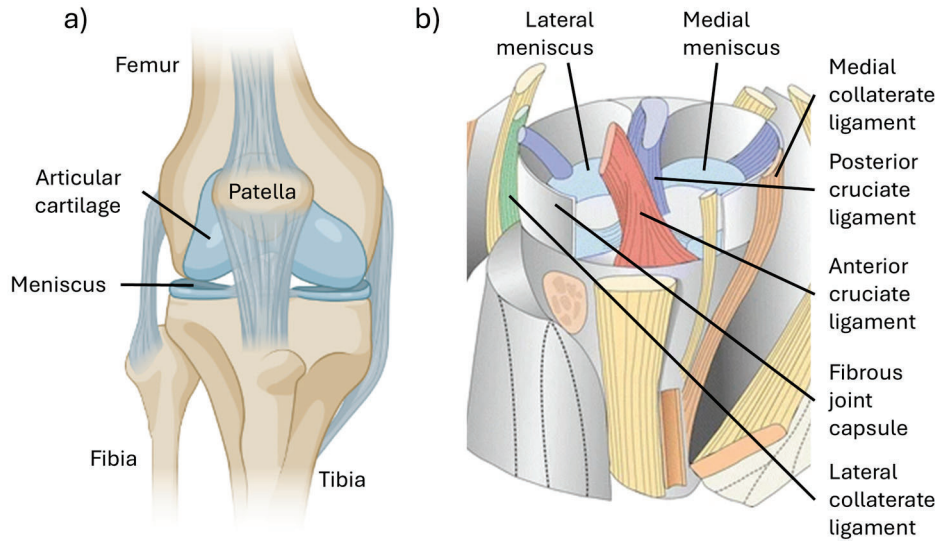

Figure 3.1: Knee joint anatomy. a) Frontal view of the human knee joint, with the major bones as well as location of the articular cartilage and meniscus labeled. b) Cross-sectional view of the human knee, showing the menisci, the cruciate and collateral ligaments, and the joint capsule. Image adapted from Hirschmann et al (7) with permission from Springer Nature.

3.1.1 Articular Cartilage

On the ends of the bones forming the knee joint sits its articular cartilage. It enables normal physiological motion of the knee, by providing a low-friction surface and the ability to withstand and transmit high loads without permanent damage. This load-bearing ability in turn arises from viscoelastic mechanical properties arising from the composition of the tissue (7, 32).

The tissue consists of 65-80% water contained within a protein matrix. This matrix in turn is composed of roughly 60% collagen (dry weight) with the remainder being proteoglycans (7). Collagen makes up the overall structure of articular cartilage, with primarily type II collagen forming a zonal fiber network. Sparsely interspersed in this network are specialized cells known as chondrocytes (7, 32). Near the surface of the tissue, the collagen fibers are arranged in parallel to form a smooth, low-friction, shear-resistant surface. This superficial zone contains a comparatively large number of chondrocytes, typically flattened and arranged with the surface. As one moves deeper into the tissue, chondrocytes become sparser in the intermediate zone, and the collagen orientation shifts into a mid-way point between being parallel and perpendicular to the surface. Finally, in the deep zone of the tissue, collagen fibers

are arranged perpendicularly to the bone interface, with chondrocytes arranged in columns following the fibers (7, 32, 33) (Figure 3.2a).

The remaining protein component of the articular cartilage is primarily made up of proteoglycans. These proteins consist of a core with attached charged glycosaminoglycan chains, which attract water molecules. This interaction contributes to the compressive resistance of the tissue both through electrostatic repulsion and by restricting the flow of water through the tissue. This combination of components and interactions results in a tissue with time-dependent mechanical response to load. When load is applied to articular cartilage, water viscously flows through the tissue, altering tissue stiffness over time and producing a viscoelastic creep and stress-relaxation response (7). As a consequence, both water diffusivity (34-36) and proteoglycan content (5, 37) are important markers of tissue health.

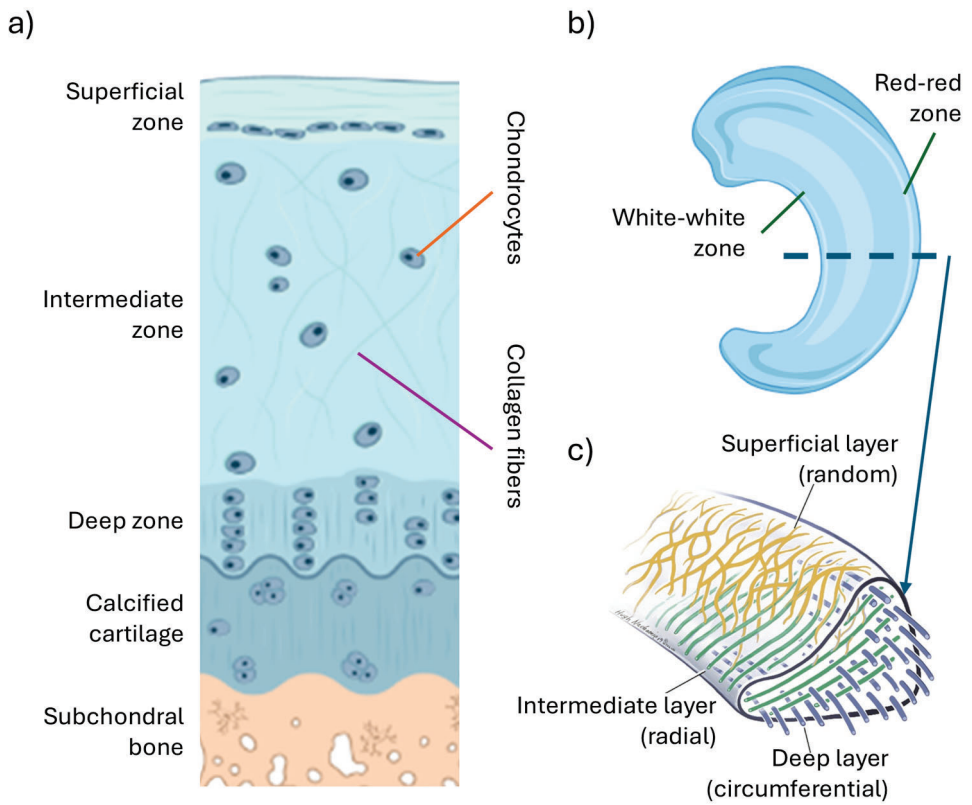

Figure 3.2: Cartilage and meniscus anatomy. a) Cross-section of the articular cartilage, showing the zonal divisions as well as organization of chondrocytes and collagen fibers. b) Diagram of the medial meniscus, showing the vascular red-red and avascular white-white zone. c) Cross-section of the meniscus, showing fiber orientation in the different layers. Image adapted from Baron et al (33) with permission from Springer Nature.

3.1.2 Meniscus

The menisci are two crescent-shaped cushions of cartilaginous tissue located between the bones of the knee joint, one in the medial and one in the lateral compartment. They are attached to each other as well as the joint's bones via several ligaments. As the menisci assist in distributing loads across the joint, provide a low-friction surface, and guide knee rotation, they are vital in reducing the stress on the articular cartilage (30). Unlike articular cartilage, the meniscus is partially vascularized, with some regions having direct access to vascular nutrient supply while others remain dependent on diffusion (30). This vascularization primarily extends into the peripheral region of the meniscus, known as the red-red zone, whereas the inner part of the crescent known as the white-white zone is entirely avascular (30) (Figure 3.2b).

Much like articular cartilage, the meniscus has a high water content (65-72%) with the majority of the dry weight being made up of collagens. Microstructurally, the structure varies between the red-red and white-white zones. In the red-red zone these collagens primarily consist of type I fibres arranged with different patterns depending on their vertical location within the tissue. In the centre of the meniscus, they follow the crescent shape of the overall structure, while re-orienting into a radial direction in an intermediate layer before forming a tight mesh in the tissue surface (Figure 3.3c). The collagen structure in the white-white zone follows a similar structure, although type II collagen plays a larger role, making up about 60% of the dry weight (30). This collagen structure is supplemented by proteoglycans, which serve a similar role as in articular cartilage, albeit being less abundant (9, 30, 38). The water retention properties of the collagen-proteoglycan matrix gives rise to the viscoelastic mechanical properties the meniscus requires to properly distribute loads within the joint (39).

3.1.3 Degeneration and Osteoarthritis

As both the articular cartilage and meniscus are sparsely cellularized and wholly or partially avascular, their healing ability is very limited (1, 4, 30, 32). Consequently, these tissues need to endure for a lifetime. While the chondrocytes perform important tissue maintenance functions, their ability to repair damage is limited which can lead to an accumulation of damage over time. Accumulated damage can eventually lead to progressive degeneration of the tissue, which culminates in the disease of OA. Corresponding illness may result when degeneration reaches the point where damage to the tissues of the knee joint causes persistent inflammation, which may lead to pain, swelling, and difficulty in movement (1, 4).

As degeneration partly results from accumulated tissue damage, the processes are associated with age and are exacerbated by various knee injuries (1, 40).

Furthermore, OA is a heavily underdiagnosed disease (41, 42) as diagnosis is primarily based on patient-reported symptoms (4). Consequently, the early stages of OA are understudied, and the dividing line between OA and normal aging can be unclear as pathophysiological signs of joint degeneration are more common with increasing age even in individuals without reported clinical symptoms (43). On the tissue level, degeneration in both articular cartilage and the meniscus primarily expresses itself as a disruption of the complex protein matrices that provide their structure and function (Figure 3.3). This process has been extensively studied and grouped into stages for classification based on histopathology, resulting in the OARSI grading scale for articular cartilage (5) and the Pauli scale for meniscus (44). These scales allow levels of degeneration to be quantified and compared between individuals and make for the basis of comparison with novel techniques.

In articular cartilage, degeneration depletes the proteoglycan content of the tissue and gives rise to several characteristic features. Initially, microscopic cracks appear at the tissue surface, eventually causing fibrillation and then deepening into larger cracks with distinct collagen fibre structures. The chondrocytes within the cartilage are also disrupted in various ways, including chondrocyte clustering, death, hypertrophy, or hypotrophy (5, 45). Degeneration of the meniscus proceeds in a similar manner, with the initially highly ordered layers of collagen fibres becoming increasingly disorganized as degeneration progresses (9, 44).

Investigation of the causes of these degenerative processes is a highly active field of research, yet the exact reasons are not fully understood. Changes in tissue biology during degeneration and osteoarthritis can be studied using a number of approaches, from classical histology (5, 43, 44), to MRI-based methods (6, 34-36, 46, 47), to contrast-enhanced X-ray approaches (48-50). Classical histology provides the highest level of detail but is restricted to imaging fixed tissue in two dimensions, losing many aspects of the physiological state. X-ray imaging can expand this into three dimensions but struggles to provide contrast within soft tissue without some method of contrast enhancement. MRI does provide three-dimensional (3D) data but has comparatively low resolution. Additionally, while MRI can probe metrics such as hydrogen density, MRI signals are heavily dependent on the chemical state of hydrogen (51), resulting in confounding factors. Consequently, the use of neutron approaches could more cleanly probe both hydrogen (and consequently water) content and motions in the tissue. Phase-contrast enhancement similarly can extend the ability of X-rays to produce clear images potentially matching histology in quality (8). As a result, the development of new investigative approaches could produce further insights into the degenerative process that were previously not possible.

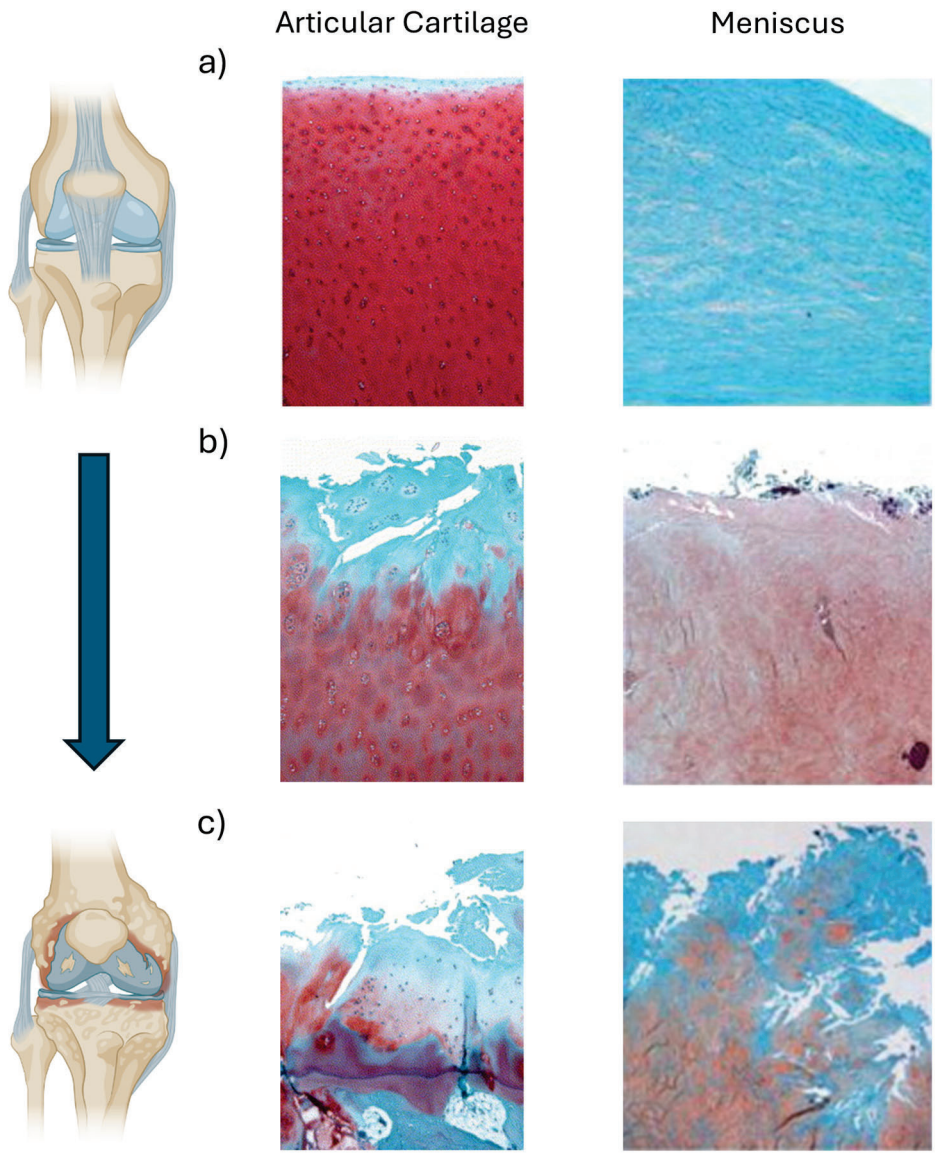

Figure 3.3: Degeneration examples. a) Histopathological images of healthy articular cartilage (OARSI 0) and meniscus (Pauli score 0) b) Histopathological images of moderately degenerated articular cartilage (OARSI 3-3.5) and meniscus (Pauli score 2 for meniscus integrity). c) Histopathological images of severely degenerated articular cartilage (OARSI 6) and meniscus (Pauli score 3 for meniscus integrity). Articular cartilage and meniscus images reprinted from Pritzker et al (5) and Pauli et al (44), respectively, with permission from Elsevier.

3.2 Neutron and X-Ray Techniques

The possibilities for characterization of cartilage and meniscus can be expanded with a number of neutron and X-ray-based techniques. These techniques are often complementary as neutrons and X-rays interact with matter in fundamentally different ways. Being electromagnetic radiation, X-rays primarily interact with the electron cloud, and X-ray interactions thus scale predictably with atomic number or material electron density. In contrast, neutrons carry no electric charge and thus primarily interact with atomic nuclei, making neutron interaction cross-sections entirely dependent on the properties of the nucleus (52). These interaction cross-sections vary widely throughout the periodic table, making neutron interactions likely in many places where X-ray interactions are unlikely, and vice versa (Figure 3.4) (53). Importantly for the study of biological tissue, neutrons are highly sensitive to hydrogen, which is nearly invisible to X-rays (52). Additionally, this nuclear dependency results in neutrons being sensitive to isotopes, allowing deuterium to be used for contrast adjustments while being chemically similar to hydrogen (13, 17).

Attenuation coefficients for thermal neutrons (cm^{-1})

1a	2a	3a	4a	5a	6a	7a	0
H							He
3.44							0.02
Li	Be	B	C	N	O	F	Ne
3.30	0.79	101.60	0.56	0.43	0.17	0.20	0.10
Na	Mg	Al	Si	P	S	Cl	Ar
0.09	0.15	0.10	0.11	0.12	0.06	1.33	0.03

Attenuation coefficients for thermal X-rays (cm^{-1}) (150 kV)

1a	2a	3a	4a	5a	6a	7a	0
H							He
0.02							0.02
Li	Be	B	C	N	O	F	Ne
0.06	0.22	0.28	0.27	0.11	0.16	0.14	0.17
Na	Mg	Al	Si	P	S	Cl	Ar
0.13	0.24	0.38	0.33	0.25	0.30	0.23	0.20

Figure 3.4: Neutron and X-ray interactions. Partial periodic table showing attenuation coefficients of thermal neutrons and X-rays. Particularly hydrogen is of interest in biological materials, being strongly attenuating for neutrons but weakly for X-rays. Image adapted from Martell et al. under Creative Commons license.

3.2.1 Neutron and X-Ray Sources

Any measurement utilizing either neutrons or X-rays requires a source of the radiation in question, with a number of options being available.

X-rays for most applications are sourced from lab sources using bremsstrahlung-based X-ray tubes (54). These sources, while often capable of high flux, are limited in that they produce a comparatively wide energy spectrum as well as incoherent and non-polarized radiation. Synchrotron sources on the other hand provide X-rays of much higher brilliance and coherence at the expense of requiring large-scale accelerator facilities. Synchrotrons operate by accelerating magnetically confined electrons around a ring and utilizing the radiation emitted when electrons pass through a bending magnet or other magnetic array intended to produce an oscillation (55) (Figure 3.5a). This process produces brilliance many orders of magnitude higher than what is possible in a lab source, enabling much faster measurements or greatly

enhancing the signal-to-noise ratio and/or resolution of many X-ray-based characterization techniques. Examples of synchrotron sources include MAX IV in Lund, Sweden (24), the Swiss Light Source (SLS) in Villigen, Switzerland (56), or the European Synchrotron Radiation Facility (ESRF) in Grenoble, France (57).

Neutrons are generally more complicated to produce, and while a number of compact neutron sources have been developed (58, 59) there are still no neutron "lab sources" available that are comparable to those for X-rays. Neutron production operates on one of two principles, either neutron emission during nuclear fission, or spallation produced as a particle impacts a heavy atomic nucleus (52, 59). Fission-based neutron sources are essentially conventional nuclear reactors optimized for neutron emission rather than power production. Spallation sources (Figure 3.5b) on the other hand use a linear proton accelerator to accelerate a stream of protons into a heavy metal target, typically lead, mercury, or tungsten. This causes a cascade reaction in which a large number of neutrons are ejected from the target nuclei. Generally, fission-based sources are more suitable to producing continuous high neutron flux, while spallation sources more suitable for production of short pulses of very high flux (59). In both cases, produced neutrons are processed through a moderating fluid (typically water or liquid hydrogen) to reach energies suitable for experiments before being directed into beamlines. For biological experiments, these energies span the cold, thermal, and epithermal spectra, an energy range from 0.025 eV – 10 keV (52, 59). Notably, these energies are substantially lower than X-ray energies, which typically range from 12 – 140 keV (60), enabling some techniques not feasible with X-rays. An example fission-based reactor source is the Institute Laue-Langevin (ILL) in Grenoble, France (61), while example spallation sources are the ESS in Lund, Sweden (25), the Swiss Spallation Neutron Source (SINQ) in Villigen, Switzerland (62), or the Japan Proton Accelerator Research Complex (J-PARC) in Tokai, Japan (63).

Generally, neutron sources will produce much lower beam intensities than X-ray sources due to the increased difficulty of neutron production. This in turn means that while neutrons are highly complementary to X-rays, neutron experiments in general have lower resolution than X-rays and take considerably more time to perform, with the most advanced neutron sources being comparable to the resolution-time performance of commonly available X-ray lab sources.

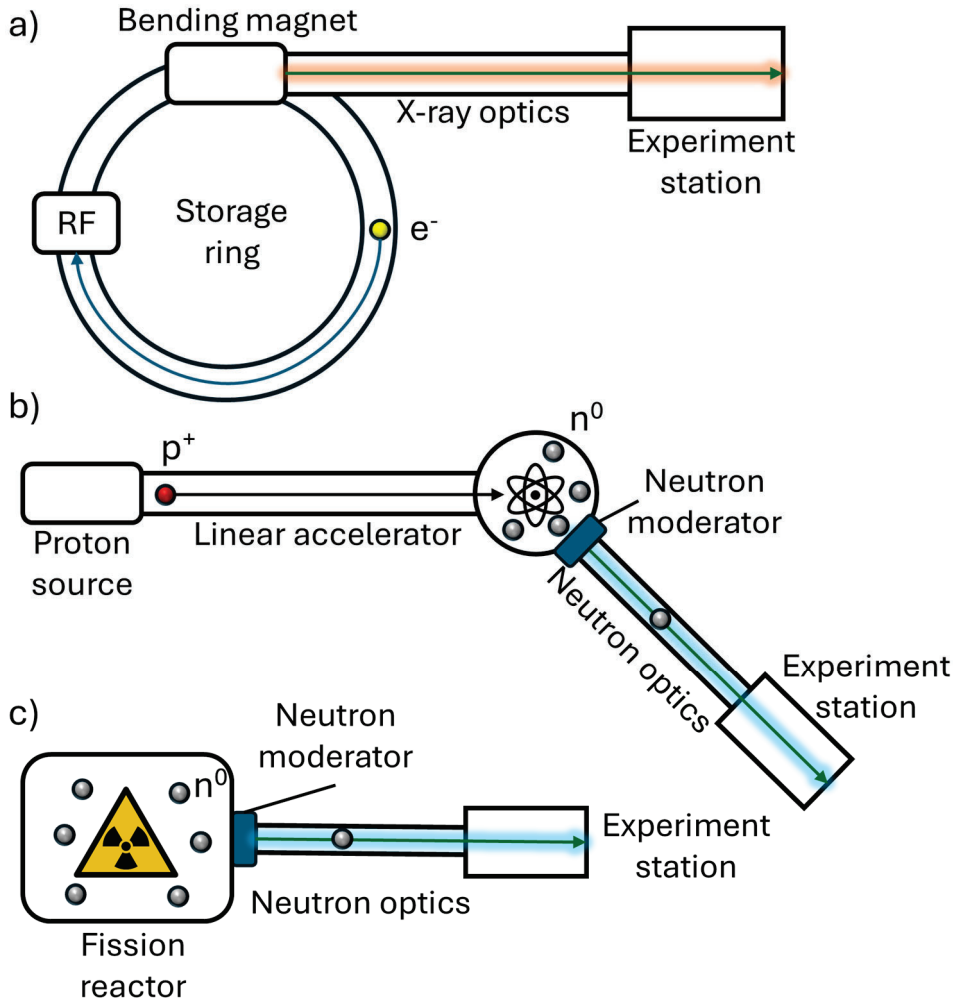

Figure 3.5: Example X-ray and neutron sources. a) Diagram of a synchrotron source, showing the ring accelerator as well as insertion devices and bending magnets producing radiation for beamlines. b) Diagram of a spallation source, showing a linear accelerator sending protons into a target to produce neutrons via spallation. c) Diagram of a reactor source, showing a fission reactor emitting neutrons which are then moderated and sent to an experiment station.

3.2.2 Computed Tomography

Computed tomography is an algorithmic method to construct a 3D volume from a series of two-dimensional (2D) radiograms. Radiograms in turn are images produced by the passage of some form of radiation beam through a sample, usually with contrast produced by the absorption or deflection of the radiation in question. These

images are then converted into a 3D volume through backpropagation, essentially deriving the shape an object must have to produce the series of projections captured (52, 64, 65) (Figure 3.6a). Tomography is used in both clinical diagnostics, lab-based research, and large-scale facility settings, with the difference of most import being the intensity of radiation available, which in turn affects possible resolutions and imaging speeds.

Attenuation contrast

The most common method of contrast in tomographic imaging is attenuation, effectively measuring the distribution of attenuation coefficients in the imaged sample in 3D (Figure 3.6b). The effect of attenuation coefficients on beam intensity is described by the Beer-Lambert law:

$$I = I_0 e^{-\mu d}$$

Where I is the resulting beam intensity, I_0 is the initial beam intensity, μ is the material-dependent attenuation coefficient, and d is the path length (65).

As X-rays primarily interact with the electrons of a material, their attenuation coefficients are typically a direct proxy for material density, providing relatively little contrast between different types of soft tissue. Chemical contrast enhancement can alleviate this issue (48), but traditionally this has made attenuation-based X-ray tomography less useful for soft tissue studies compared to hard tissue like bone.

Neutron attenuation contrast on the other hand is highly sensitive to hydrogen. Consequently, it provides strong contrast between materials with different levels of hydration, something which has been applied extensively to study water transport in materials ranging from rocks to plant tissues (14, 15, 66, 67). Furthermore, the ability for neutrons to penetrate many denser materials allows for visualizations not possible with X-rays, such as bone ingrowth into metallic implants (68-70). Finally, the factor seven difference in neutron attenuation between regular and heavy water allows heavy water to be used as a contrast agent, which due to its chemical similarity with regular water has a much lower impact on the material studied than other forms of chemical contrast enhancement. Imaging in combination with water-heavy water exchange is key to many neutron tomography applications such as studying water exchange in bone (17, 18), plants (14, 15) or other materials (67). Capabilities range from imaging total exchange of water at high (<20 μm) resolution (18), to capturing rapid motions of water with fast (10s/tomogram) lower-resolution (~200 μm) tomographies (15). Consequently, a wide range of applications for studying water in soft tissue ought to be possible.

Examples of neutron tomographic imaging beamlines used in the current thesis include NeXT-Grenoble at ILL, France (71) and ICON at SINQ, Paul Scherrer Institut (PSI), Switzerland (72) (Figure 3.3). Further examples of beamlines offering this capability include IMAT at the ISIS Neutron and Muon Source, UK (73), BL-10 Venus at the Spallation Neutron Source (SNS), USA (74), or BL22 RADEN at J-PARC, Japan (75).

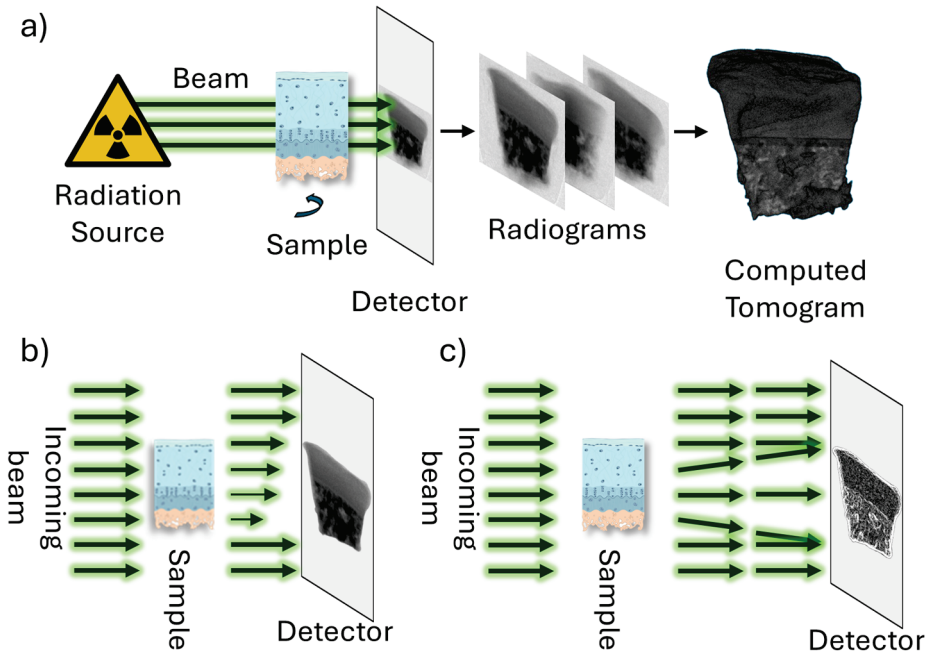

Figure 3.6: Schematic of tomography. a) Schematic representation of tomography. A radiation beam is passed through a rotating sample, producing a series of radiograms from which a 3D tomogram can be computed. b) Attenuation imaging, capturing reduction in intensity in the beam passing through a sample. c) Propagation-based phase-contrast imaging, capturing phase changes induced by edges of the sample or between materials within through interference during propagation.

Phase-contrast

An alternative to attenuation is measuring the phase shift resulting from the complex refractive index of a material that the radiation is passing through. Typically, the information encoded in the phase change is highly complementary to that produced by absorption, particularly highlighting edges between materials of similar absorptive properties (76, 77) (Figure 3.6c). While the phase shift cannot be directly measured, it can be retrieved through a number of indirect methods such as propagation-based imaging (77, 78) or grating interferometry (76). Propagation-based imaging is the most commonly used approach at synchrotron sources, as their highly coherent

beams make it relatively simple to utilize. The detector is moved further away from the object to be imaged, allowing the beam to propagate further to enhance the effect of small phase shifts, before being detected. This in turn allows the phase-shifted components of the beam to interfere, producing detectable amplitude differences particularly at the edges between materials with different refractive indices but similar absorption (79).

For X-rays, this technique produces images with substantially higher contrast in soft tissue than X-ray attenuation (77). This technique has seen widespread use within biological imaging in recent years, often being described as "virtual histology" for its ability to generate images of similar quality to histological slices observed by light microscopy (8, 76). It has been applied to a number of purposes such as studies of neuronal tissue (80), intervertebral discs (81), Achilles tendon (82, 83), and meniscus (9, 11), although its application to articular cartilage is still rather sparse (10, 11). In all these tissues, phase-contrast imaging has been able to visualize fibre structures as well as cells with resolutions on the order of 1-10 μm. Previous work on cartilage has shown high-resolution 3D visualization of the tissue (10) but has been highly limited in its ability to draw any conclusions about degeneration due to a small sample size.

Examples of beamlines with phase-contrast imaging capabilities used in this thesis are ForMAX at MAX IV, Sweden (26) and TOMCAT at SLS, Switzerland (84). Other examples include I13-2 at the Diamond Light Source (DLS), UK (85), BM18 at ESRF, France (86) or P05 at PETRA III, Deutsches Elektronen-Synchrotron (DESY), Germany (87).

3.2.3 Quasi-Elastic Neutron Scattering

Quasi-elastic neutron scattering (QENS) is a technique which utilizes the relatively low energy of cold and thermal neutrons to probe low-energy motions in materials (19). Notably, these neutrons have energies in the meV range while simultaneously having wavelengths in the 1-10 Å range, corresponding to molecular distances. Combined with the fact that neutrons only interact through nuclear and (negligible in biological tissues) magnetic interactions, this allows for spectroscopic measurements of motions in a material. In principle, one measures momentum transfers and energy shifts of neutrons scattered by a material (Figure 3.7). These neutron spectra can then be fit to models relating particular molecular motions to the relationship between momentum transfer and energy shift distributions (19, 20).

As hydrogen scatters neutrons quite powerfully, any QENS signal in a biological or otherwise water-rich system will predominantly probe hydrogen motions, which in turn correspond to the motion of water or biomolecules within a system. Notably, this allows for the study of water diffusion on a nano- to picosecond timescale (20),

as well as several molecular motions in protein systems (21). Studies on more complicated systems are also possible, performing feats such as distinguishing water populations with different diffusivities. Within biological tissues or materials, this has been applied to study diffusivity in bovine brain tissue (22) or investigating the connection between strain and protein diffusion in silk fibres (23) but remains unexplored in musculoskeletal tissues. As soft knee tissues depend on diffusivity for their nutrient supply and mechanical properties, their water and protein diffusivities are of substantial interest for understanding the tissue.

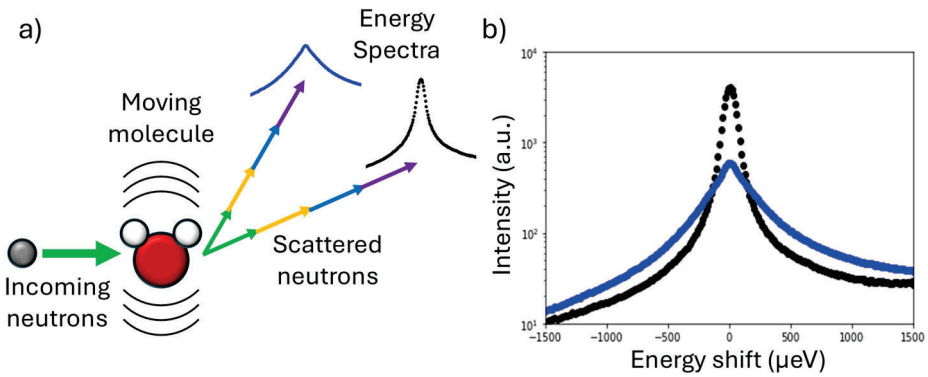

Figure 3.7: Quasi-elastic neutron scattering. a) Schematic representation of QENS. Neutrons interact with a moving molecule, and are scattered with small changes in energies, producing spectra of energy changes at specific scattering angles. b) Examples of quasi-elastic spectra at two different scattering angles.

3.3 Complementary Imaging

A number of other imaging techniques complement the data that can be acquired with X-rays and neutrons, with the two most important ones being histological microscopy as well as magnetic resonance imaging. These techniques provide a state-of-the-art for both characterization of articular cartilage and meniscus tissue, and their alterations during degeneration, against which novel approaches can be compared.

3.3.1 Histology

Histology forms the gold standard for 2D imaging throughout the biomedical field. For histological imaging, tissue is fixed using formaldehyde and then sliced into thin sections before being stained with histochemical agents (37). The two primary staining protocols used for articular cartilage and meniscus are hematoxylin-eosin (H&E) as well as Safranin-O and Fast Green (Saf-O). H&E primarily stains nuclei

and secondarily the collagen matrix, primarily visualizing cell morphology. Saf-O in contrast primarily stains for proteoglycans, visualizing their relative content throughout the tissue. These stained tissue slices are then imaged using conventional light microscopy.

In soft knee tissue research, these histological images form the basis for standardized assessment systems of degeneration in the articular cartilage (5) as well as the meniscus (44). Examples of these images can be seen in figure 3.3. These systems employ a number of criteria for evaluating tissue degeneration. The OARSI scale examines the level of cartilage surface damage, changes in cell morphology, proteoglycan depletion, and eventual bone alterations at later stages (5). It ranges from 0 (healthy cartilage) to 6 (bone deformation after denudation of the bone). The Pauli score system operates in a similar manner on meniscus, deriving a composite score from separate scorings of the status of the meniscus surface, meniscus cellularity, collagen fibre organization, and matrix staining indicative of proteoglycan changes. These systems allow for comprehensive evaluation of tissue degeneration status and its relationship to other parameters such as patient age (43), forming the basis for comparison to other investigations of tissue health.

3.3.2 Magnetic Resonance Imaging

MRI is another important technique for the imaging of articular cartilage and meniscus, both due to its ability to capture 3D information and capability for *in vivo* use (Figure 3.8a) (88). Clinical MRI is primarily used to detect macroscopic tissue damage (40, 89, 90), but can also be indicative of changes in biochemical composition (6, 91).

To produce images in MRI, a strong magnetic field is applied to the tissue to be imaged, aligning the magnetic moments of the hydrogen atoms present within to the field. The interaction of these magnetized hydrogens with a radiofrequency signal can then be used to detect both the strength of the signal (M0, from the present amount of magnetizable hydrogen) as well as the time required for magnetization to return to a ground state after the magnetic field is removed (relaxation time, T1 and T2). Applying a gradient to the magnetic field additionally allows for the spatial localization of the signal, producing an image (51). Using the different relaxation times, one can distinguish between different types of soft tissue as well as differences in tissue biochemistry (6, 51, 91).

MRI also allows for direct study of hydrogen (and therefore water) diffusion in tissues (Figure 3.8c). By applying two radiofrequency pulses that would cancel out in the absence of motion it is possible to detect diffusion occurring in the millisecond-range interval between pulses (92). This diffusion-weighted imaging can then be extended by performing it in multiple directions, producing a tensor containing anisotropic information about the diffusion, a process known as diffusion-tensor imaging (93, 94). This method has in turn been used extensively to study diffusivity in both articular cartilage (34-36, 95) and meniscus (96).

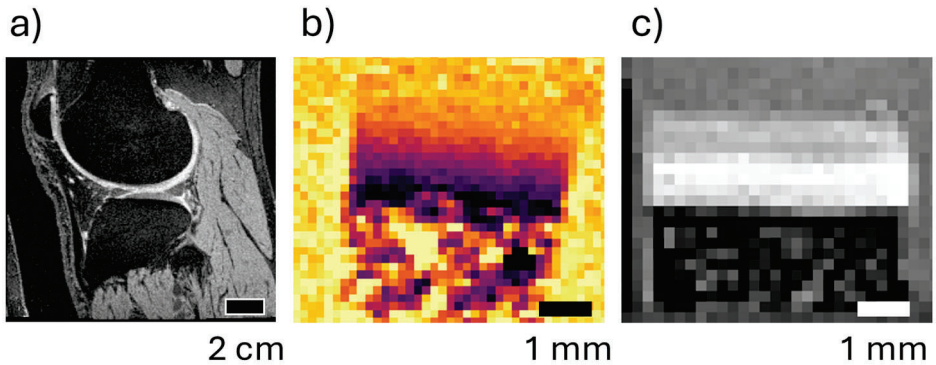

Figure 3.8: MRI examples. a) Clinical MRI of a human knee in the sagittal plane, adapted from Gaj et al (88) with permission from Wiley. b) M0 (proton density) MRI image of a human articular cartilage plug adapted from B Wrammerfors et al (Study II). c) Diffusion-weighted MRI image of a bovine articular cartilage plug adapted from Study III.

4 Methods

This chapter first describes the tissue samples used within the thesis, then the principal methods used for tissue characterization together with the state of the art techniques used as a complement, followed by data analysis approaches.

4.1 Samples

Bovine and human tissues were used throughout the thesis work. In all instances, medial femoral cartilage or medial meniscus was chosen, from the human knee joint or the analog bovine joint.

4.1.1 Human articular cartilage (Study I-II)

Human articular cartilage samples were collected from the MENIX biobank (Skåne University Hospital, Region Skåne, Sweden, ethical approval as per Dnr 2015-39, 2016-865, and 2019-00323). The majority of samples (n=49, 24 males and 25 females) originated from donors without known clinical knee OA, ranging in ages from 18-85. An additional 4 samples originated from patients undergoing total knee replacement surgery due to advanced knee OA (ages 61-75, all female).

Samples were either drilled into ~4 mm diameter circular plugs of cartilage on bone (Study I) or cut into equivalently sized rectangular plugs using a diamond saw (Study I and II). For study I, the majority of samples were kept frozen in an untreated state while a smaller amount were fixed in formaldehyde but kept hydrated as part of the requirements for study II. Adjacent tissue from all samples was taken and prepared for histological staining and microscopic evaluation as described in (43). Examples of sample preparation can be seen in figure 4.1a-c.

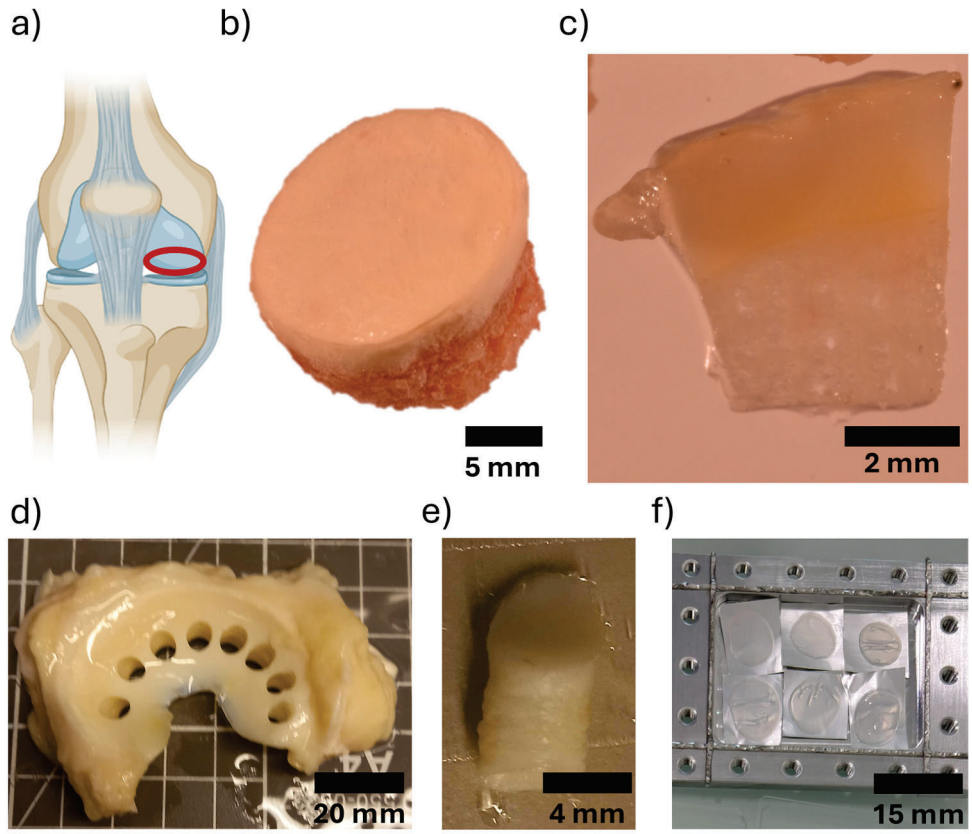

Figure 4.1: Sample preparation. a) Sampling site for human samples in the knee joint (medial femoral condyle). b) Example of a raw sample before cutting. c) Example rectangular sample plug after cutting. d) Bovine medial meniscus with plugs extracted. e) Example bovine meniscus plug after extraction. f) Cryotomed slices of bovine cartilage in QENS sample canister.

For study II, samples were separated into four different groups in order to test the effects of various preparation methods on neutron imaging. Compared were untreated samples (n=2), unfixed samples immersed in D_2O-based PBS (n=4), fixed ethanol-dehydrated and air-dried samples (n=4), and fixed samples in ethanol (n=2). Additionally, 15 samples were fixed and kept hydrated in D_2O-based PBS in order to meet facility requirements for human tissue for the follow-up imaging experiment.

Hydrated samples were kept frozen at -20C prior to and between imaging experiments, with longer-term storage at -80C. Non-hydrated fixed samples were kept refridgerated at 8C.

4.1.2 Bovine articular cartilage and meniscus (Study III-IV)

Bovine tissues for study III were prepared in a similar manner as outlined for human tissues. Whole bovine knee joints were sourced from a local slaughterhouse. 4-5 mm plugs of cartilage on bone were drilled from the medial femoral condyle, and same-size circular plugs were taken from the medial meniscus using a biopsy punch (Figure 4.1d-e). All samples were kept untreated in conventional PBS, and frozen at -20C until usage.

For study IV, disks were cut from bovine femoral condyles, aiming for cartilage that was as flat as possible. From these disks, 100 μm tissue slices were cut via cryotome following the cartilage surface direction. These slices were placed on aluminium foil on microscope slides and then kept frozen at -20C until usage (Figure 4.1f).

4.2 Phase-contrast synchrotron tomography (Study I)

Phase-contrast imaging was performed at the TOMCAT beamline at PSI, Switzerland (84) and the ForMAX beamline at MAX IV, Lund (26). For the bulk of the imaging, tomograms were taken at TOMCAT at 2.75 μm isotropic voxel size keeping the samples in phosphate-buffered saline (PBS) in a custom 3D-printed sample holder (figure 4.2a). Projections were processed through a dynamic flat-field correction algorithm (97) before tomograms were reconstructed using Paganin phase retrieval and the Gridrec algorithm (78, 98).

Two samples were later cut into smaller pieces (diameter ~1 mm) and re-imaged at 0.65 μm voxel size at ForMAX. These images were reconstructed using TomoPy (99) with static flat-field correction and a Paganin filter. Full imaging parameters can be found in table 4.1 and imaging setups can be seen in figure 4.3a-b.

Table 4.1: Imaging parameters for phase-contrast synchrotron experiments.

Experiment	TOMCAT	ForMAX
Voxel Size	2.75 μm	0.65 μm
Field of View (FoV)	5.54 x 3.85 mm^2	1.7 x 1.4 mm^2
X-ray Energy	21 keV	16 keV
Propagation Distance	40 cm	5 cm
Exposure Time	9 ms	40 ms
Projections	4000/180°	1800/180°
Total Imaging Time	40 s	80 s

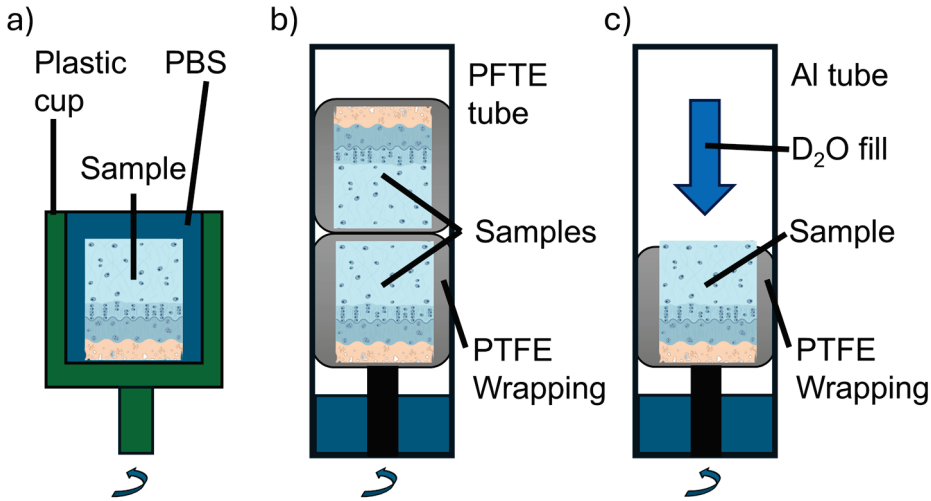

Figure 4.2: Imaging setups. a) Sample submerged in PBS in plastic cup for phase-contrast imaging (study I). b) 2 samples wrapped in PFTE in sealed tube with water pocket to retain moisture (study II). c) Sample wrapped in PFTE with open top for filling with D_2O for diffusion imaging (study III).

4.3 Neutron tomography (Study II-III)

Neutron imaging was performed at the NeXT-Grenoble beamline at ILL, France (71) as well as the ICON beamline at PSI, Switzerland (72).

For static imaging of human specimens (Study II), samples were wrapped in polytetrafluoroethylene (PFTE) tape and placed either in sets of two in a PFTE tube (at NeXT, figure 4.2b) or in sets of three in an aluminium tube (at ICON) with a pocket for liquid in the bottom. This design was chosen to prevent dehydration during long imaging times while avoiding direct placement of the sample in high-attenuation, low-contrast water or heavy water. Imaging was performed at 7.5 μm voxel size (at NeXT) or at 13.5 μm voxel size (at ICON). Volumes were reconstructed using Xact commercial software (RX Solutions, at ILL) or MuhRec open-source software (at ICON)(100). Full imaging parameters can be found in table 4.2 and imaging setups are pictured in figure 4.3c-d.

Diffusion imaging of bovine tissues was performed at NeXT. Here a similar tube as with the static experiments was used, albeit with just a single sample. The samples were wrapped in PFTE around the sides, leaving the top open to allow heavy water to diffuse in (figure 4.2c). An initial static tomogram was taken, then the tube was manually filled with heavy water PBS. Subsequently, continuous tomograms were

taken over the course of 2 hours (for cartilage) and 8 hours (for meniscus). Images were taken at 14.3 μm isotropic voxel size with differing exposure times and projections in order to achieve required time resolutions (5.625 min per tomogram for cartilage, 22.5 min for meniscus), full parameters can be found in table 4.2. Reconstruction was performed in XAct.

Table 4.2: Imaging parameters for neutron tomography experiments.

Experiment	Study II NeXT Cartilage	Study II ICON Cartilage	Study III NeXT Meniscus	Study III NeXT Cartilage
Voxel Size	7.5 μm	13.5 μm	14.3 μm	14.3 μm
FoV	14x14 mm^2	27x27 mm^2	14x14 mm^2	14x14 mm^2
L/D	333	343	333	333
Scintillator	10 μm gadolinium	20 μm gadox	10 μm gadolinium	10 μm gadolinium
Exposure	5 s avg 3	90 s	0.5 s avg 3	0.25 s avg 3
Projections	1216/360°	625/360°	900/360°	450/360°
Imaging Time	5 h	16 h	22.5 min	5.625 min

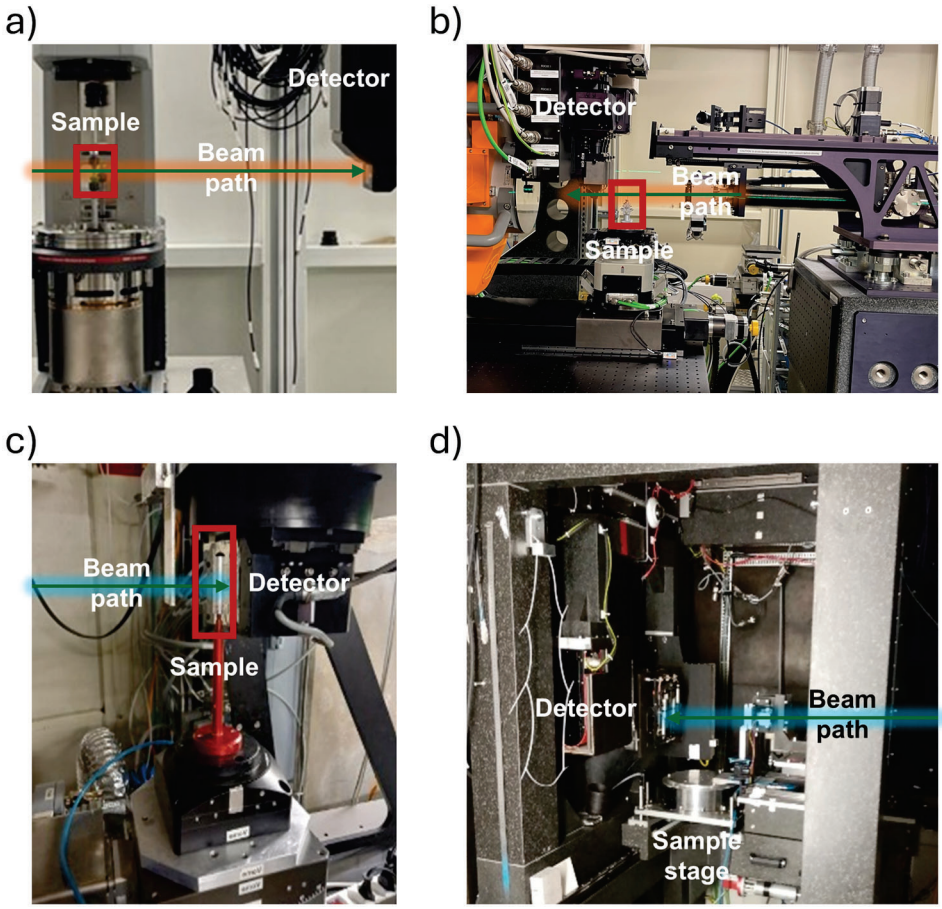

Figure 4.3: Imaging beamlines. Top row: synchrotron phase-contrast imaging beamlines TOMCAT (a, study I) and ForMAX (b, study I). Bottom row: neutron imaging beamlines ICON (c, study II) and NeXT (d, studies II-III). Sample or sample stage location, detector position, and beam path is labelled in each setup.

4.4 Quasi-elastic neutron scattering (Study IV)

QENS was performed in two separate experiments at ILL, France. First a broad (meV energy range) QENS measurement was carried out at the IN5 time-of-flight spectrometer to quantify bulk water diffusion. Sample sets of 100 μm thick cartilage slices were taken from the intermediate and deep zones, respectively, of a single bovine femoral condyle. Both sample sets had QENS spectra measured at 310K (= 37C), with the deep zone cartilage having additional measurements taken at 280, 250, and 220K.

A complementary narrow measurement (μeV range) was carried out at the IN16B backscattering spectrometer to quantify protein motions and potentially present slow water motions. Samples from the superficial, deep, and intermediate zones were prepared as above. Initially, and inelastic fixed-window scan was taken to identify temperatures of interest. Then QENS spectra were taken for each sample at 310, 278, 268, 258, and 248 K. Data from both experiments was reduced using Mantid (101) in preparation for analysis.

4.5 Complementary techniques

State of the art complementary histology, MRI and X-ray tomography were used on the same samples throughout the thesis work to provide standard information for comparison.

4.5.1 Histology (Study I-II)

Adjacent tissue from all the imaged human samples was taken and prepared for histology as presented by Sjögren et al. (102). Samples were fixed in 4% formaldehyde followed by ethylenediaminetetraacetic acid (EDTA) decalcification, ethanol dehydration, and paraffin embedding.

Separate sections from each sample were stained with Hematoxylin and Eosin (H&E) for cell visualization or Safranin-O and Fast Green (Saf-O) as standard for OARSI osteoarthritis grading (5). Saf-O sections were then assessed for OARSI grades by two rounds of consensus grading (102).

4.5.2 MRI (Study II-IV)

Two different sets of complementary MRI measurements were performed. The unfixed human samples which were neutron imaged in Study II (n=6) were imaged for T1 and T2* maps as well as T1-corrected M0 images. Imaging was performed at Lund University Bioimaging Center with a 9.4 T MRI (Bruker BioSpec Avance III) using a RARE (103) and 2D Ultrashort Time Echo (104) sequence with a 150 μm pixel size in 300 μm slices.

For the bovine samples imaged in Study III diffusion tensor imaging was performed at the NMR laboratory at Physical Chemistry, Lund University with a 11.7 T NMR machine (Bruker Neo 500) at 200 μm isotropic voxel size. Images were acquired with a 3D diffusion-tensor imaging (DTI) protocol, with 1 b_0 measurement and then 6 non-colinear diffusion-weighted measurements at b = 550 s/mm2 and an echo time of 15.35 ms, with a gradient duration of 2.5 ms and separation of 7.5 ms.

4.5.3 Conventional X-ray tomography (Study II-III)

All non-dried samples from Study II were imaged with conventional X-ray tomography at the 4D imaging lab, Lund University, for visual comparison to the neutron images. Imaging was performed using a RX Solutions EasyTom150, acquiring tomograms at 50 kV using 992 projections over a full rotation with a 32x32 mm FoV and 24 μm isotropic voxel size, yielding similar true resolution as the neutron images.

In Study III, X-ray imaging was performed directly after neutron imaging at the NeXT beamline (71), primarily for the purpose of segmentation. X-rays were taken after the conclusion of the diffusion experiment, with the setup of NeXT enabling imaging without direct sample manipulation, consequently allowing for co-registration of X-ray and neutron images. These tomograms were acquired at 100 keV using 1216 average-of-5 projections with 0.11s exposure time over a full rotation, with a source-to-object distance of 32 mm, source-to-detector distance of 516 mm, isotropic voxel size of 7.15 μm, and a FoV of 15x15 mm.

4.6 Data analysis

Data analysis primarily consisted of image analysis combined with quantitative analysis of reduced data derived from the images. Analysis was performed with a combination of software, including Fiji (105), Dragonfly (106), QuPath (107), Ilastik (108), Mantid (101), and custom MATLAB and Python scripts.

4.6.1 Tissue segmentation (Study I-III)

All three imaging studies involved segmentation of soft tissue from background and bone. In study I, phase-contrast volumes were first cropped into rectangular volumes of interest (VOIs) and then segmented by detecting the largest vertical grey value gradients in the top and bottom half of the volume.

Neutron volume segmentation was more complex as the contrast between cartilage and bone is minimal in D_2O-soaked samples. In study II, samples were first separated from the background and marrow tissue with a k-means clustering algorithm. A plane was then fitted to the top of the marrow phase and used to approximate the bone-cartilage interface. The tissue segmentation process is schematically described in figure 4.4. For study III, the subsequent X-ray imaging simplified the process. The background was segmented through simple thresholding followed by another step thresholding away the bone based on the registered X-ray volume.

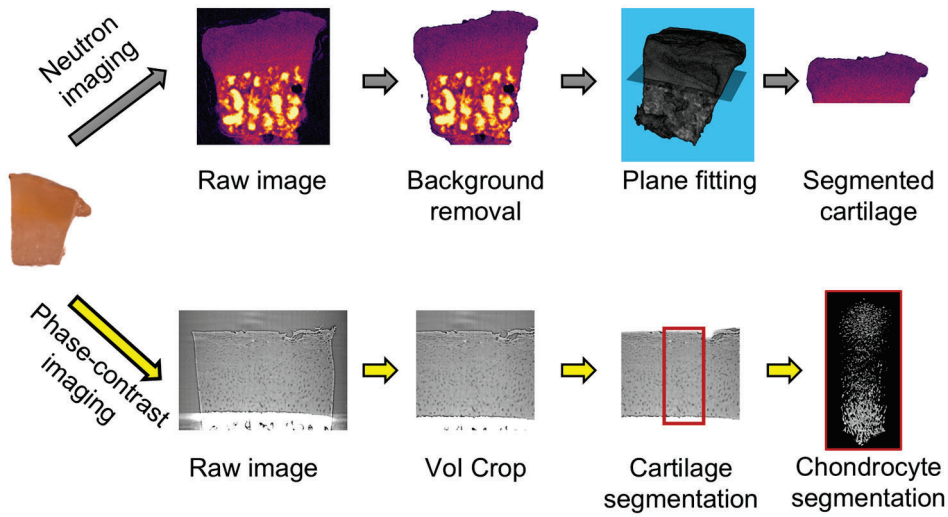

Figure 4.4: Tissue segmentation schematic. Top row: Neutron image segmentation, starting with the raw image, then removing the background via k-means clustering, then fitting a plane to the top of marrow and finally segmenting cartilage based on said plane. Bottom row: Phase-contrast image segmentation, starting with the raw image, cropping to the VoI used for analysis, segmenting out the cartilage and proceeding to chondrocyte segmentation.

4.6.2 Cell segmentation and analysis (Study I)

Within the segmented cartilage from the phase-contrast images from TOMCAT, chondrocytes were segmented from the extracellular matrix using an adaptive threshold algorithm, tuning the parameters by referencing the higher-resolution ForMAX data. Segmented bodies were then smoothed through image opening to match plausible cell shapes. Finally, they were filtered for size, excluding too-small or too-large volumes as likely noise, artefacts, or non-cell structures. An example of cell segmentation and subsequent parameter tuning can be seen in Figure 5.5.

From the segmented bodies a number of metrics were extracted and normalized to the cartilage thickness. Cell density was computed as cell volume divided by total

tissue volume. Aspect ratio and angular orientation of cell clusters was extracted with the MATLAB regionprops algorithm. These cell properties were then averaged across the same normalized depths to produce profiles for plotting and statistical modelling.

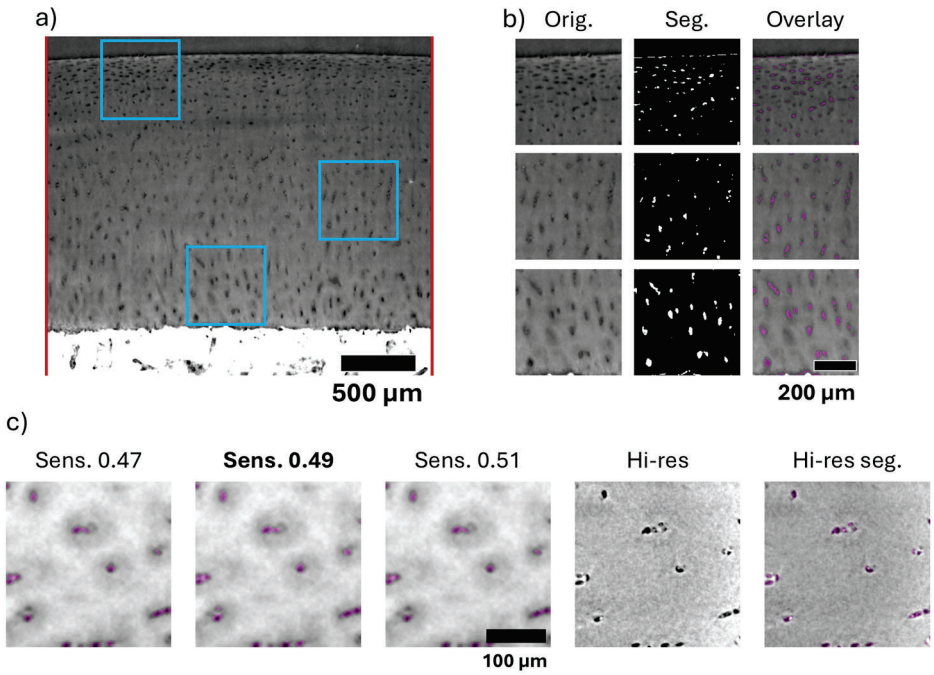

Figure 4.5: Cell Segmentation. a) Phase-contrast volume cropped to analyzed VoI, with subvolumes marked. b) Marked subvolumes with cell segmentation. c) Example of cell segmentation tuning, showing the same TOMCAT volume with three different segmentation sensitivities on the left, and a segmented higher-resolution ForMAX volume of the same region on the right.

Statistical associations between cell properties and OARSI grade were tested using a set of linear mixed models. OARSI grades were set to the fixed variable, one cell property was set as the response variable, and then tissue layer (superficial, intermediate, or deep) and sample ID as nested random variables. Correlation coefficients between OARSI grade and each cell property by layer was then extracted.

4.6.3 Histology comparison (Study I-II)

Aside from OARSI grades, histology comparisons were used both for cell properties in study I and hydrogen density versus proteoglycan content in study II.

For cell property comparisons, three H&E-stained sections were chosen from each sample, capturing as much tissue as possible while avoiding visible damage from the sectioning process. Cells were then segmented using a neural-network-based pixel classification algorithm implemented in the Ilastik software (108). Subsequently, they were analyzed for the same properties as described in the previous section but in 2D. These properties were then averaged across normalized depth in all three sections to produce similar profiles for plotting as described above. Histology cell data was also subject to the same statistical modelling as described for the XRT volumes above.

For comparison of proteoglycan concentration to hydrogen density, a similar process was carried out with the Saf-O sections. Color intensity of the Saf-O stain was extracted using QuPath before computing gradients of relative Saf-O intensity using MATLAB. Averaged points of Saf-O intensity and hydrogen density at the same depth of cartilage were then compared to determine correlation.

4.6.4 Hydrogen density profiles (Study II-III)

Hydrogen density is approximated by the attenuation in neutron imaged cartilage and meniscus volumes. This density was computed by averaging normalized columns and rows to produce vertical and radial gradient profiles, respectively. Additionally, for study III real depth gradients were also calculated by starting at the cartilage surface and averaging the grey values at the same pixel distance from the surface. To avoid artifacts from variable tissue thickness, these real-depth profiles were cropped to the median thickness of the sample.

4.6.5 Water concentration computations (Study III)

In study III, to quantify diffusion rate, relative water to heavy water concentrations were computed from neutron attenuation. The initial volumes as well as final volumes (for cartilage) or a reference volume of pure heavy water (for meniscus) were used as references. For each time step, the grey value in each voxel after a median filter and a factor 4 downscaling was compared to these two reference values to determine the heavy water concentration. Averaged gradients of these concentrations were then plotted both across depth and time, and used as the basis for modelling diffusion coefficients.

4.6.6 Diffusion model fitting (Study III-IV)

In Study III, concentration profiles derived from neutron tomography volumes were used to create finite element models of the diffusion process based on Fick's law (109, 110). In cartilage, the diffusion coefficient was assumed to follow a pattern of linear decrease through the superficial and intermediate zones while being constant in the deep zone based on MRI result. In meniscus, the diffusion coefficient was modelled as uniform. Diffusion coefficients were estimated by minimizing the normalized root mean square error between experimental and modelled concentrations.

In Study IV, diffusion was modelled using a Singwi-Sjölander jump diffusion model (19, 111). Lorentzian distributions were fitted to QENS spectra at different momentum transfers Q. The width Γ of said Lorentzians were then plotted against Q^2, allowing for fits to be made to the Singwi-Sjölander model in order to estimate the diffusion coefficient.

5 Results

This chapter describes the main outcomes of the thesis, organized based on the information that could be obtained by the various techniques. The first two sections present the tissue attributes most clearly visualized by phase-contrast synchrotron and attenuation-contrast neutron imaging. The next section presents the results of applying these imaging techniques to the study of degeneration, followed by the final section discussing applying neutron techniques to the study of water dynamics.

5.1 Chondrocyte distribution (Study I)

Phase-contrast enhanced synchrotron X-ray tomographic imaging in Study I clearly visualizes the organization of chondrocytes in articular cartilage (Figure 5.1a), enabling subsequent evaluation of degeneration-related changes. Particularly in healthy samples, distinct differences in organisation are visible between superficial, intermediate, and deep zone cells. The flattened alignment of surface cells with the surface and columnar organization of deep zone cells are both clearly visible (Figure 5.1d-f). Intermediate cells are sparser and somewhere between the two. All visualizations are fully three-dimensional, with 3D renderings (Figure 5.1c) allowing one to avoid artefacts inherent in 2D visualizations. Histology images (Figure 5.2) show more cell detail, although similar cell detail could be achieved with higher resolution phase-contrast tomography, albeit at the cost of a smaller field of view (Figure 5.2).

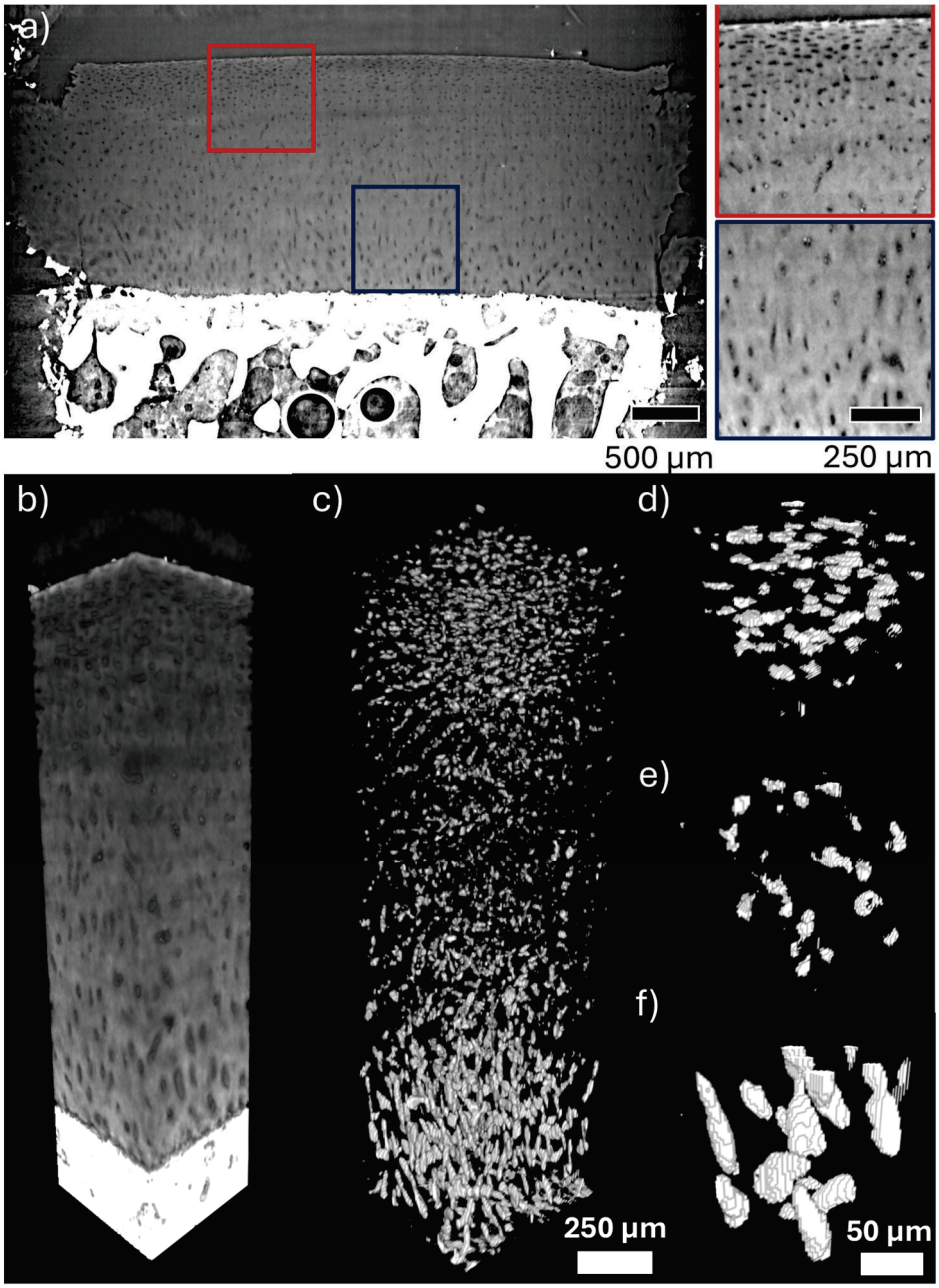

Figure 5.1: Chondrocyte Organization. a) Tomogram slice with zoom regions showing chondrocyte distribution. b) 3D rendering of a VoI from the same tomogram. c) 3D-rendering of segmented cells. d-f) Zoom regions of superficial (d), intermediate (e), and deep zone (f) chondrocytes. All images from the same donor (OARSI 0, 18F).

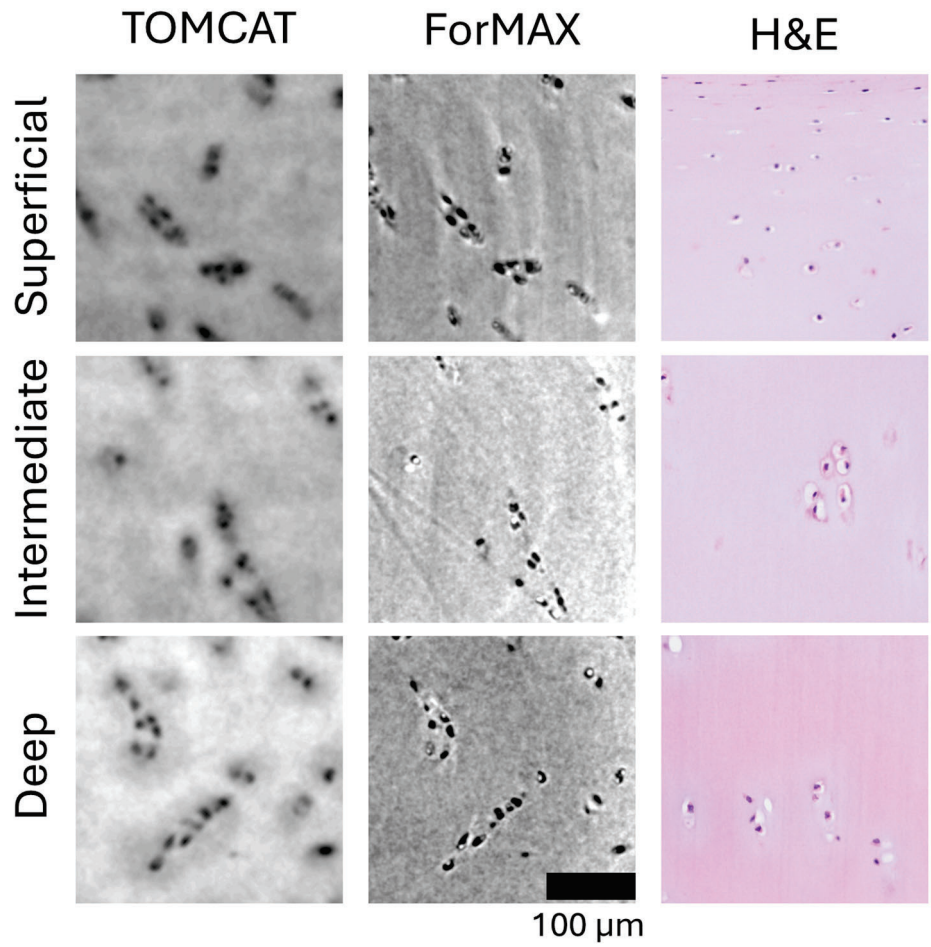

Figure 5.2: Chondrocyte visualization. Comparison between TOMCAT tomogram slices (left) and higher-resolution ForMAX tomogram slices (middle) of the same subvolumes in the superficial, intermediate, and deep zones of cartilage. H&E histology images of chondrocytes from an adjacent tissue sample from the same donor is shown for comparison at the same magnification (right). Note that tomogram slices are parallel to the tissue surface while histology is perpendicular.

5.2 Tissue hydrogen density and water content (Study II-III)

Pilot neutron imaging of untreated human articular cartilage (Study II) revealed uniform hydrogen density in hydrated tissue with a sharp contrast between cartilage and bone (Figure 5.3a). Removing the contribution of tissue water via replacement with D_2O revealed a clear increase in attenuation and consequently hydrogen density of the matrix itself towards the deep zone of the cartilage. Consequently, D_2O treatment provided the most information about the tissue matrix and its integrity.

However, the contrast with bone was minimal in these samples, indicating similar hydrogen densities in deep zone cartilage and bone.

This ability of neutron imaging to reveal hydrogen density in the tissue with and without the contribution of tissue water enabled both the study of degeneration-related changes in matrix density (see next section) and later visualization of diffusion (Study III). Sequential tomograms of diffusion into bovine articular cartilage and meniscus clearly visualize macroscopic water diffusion into the tissue (Figure 5.3b).

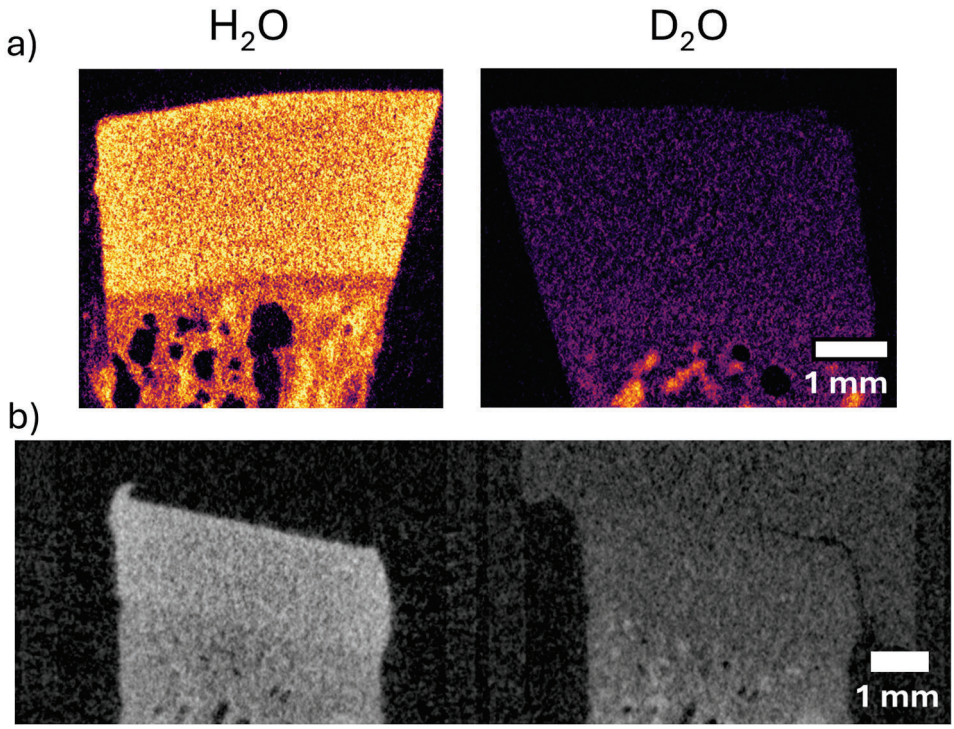

Figure 5.3: Visualization of Matrix Hydrogen Density. a) Comparison neutron tomogram slices of two human articular cartilage samples from the same donor (42M, OARSI 1), one hydrated with H_2O, the other with D_2O. b) Neutron tomogram slices of bovine articular cartilage before and after 2 hours of D_2O diffusion.

5.3 Degeneration-related changes in cells and matrix (Study I-II)

In addition to cell organization visualization, signs of matrix degeneration are clearly visible in synchrotron images from Study I. Loose surface fibres as well as deeper cracks and matrix loss are visible alongside changes in cell organization such as clustering (Figure 5.4a). Neutron images from Study II also display signs of degeneration, mainly as variations in the density of the matrix (Figure 5.4b-c).

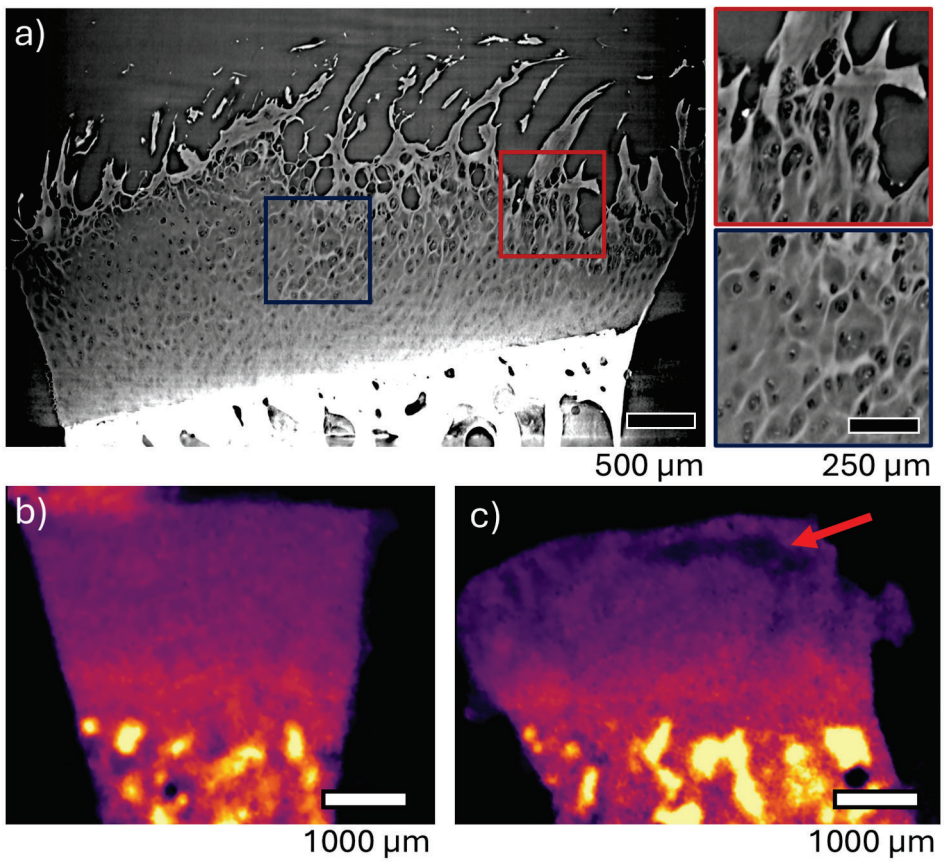

Figure 5.4: Visualization of degenerative changes. a) Phase-contrast tomogram slice of a degenerated sample from a TKR patient (71F, OARSI 4.5), with zoom regions clearly showing fibrillation and altered cell properties. b) Neutron tomogram slice from a healthy donor (32F, OARSI 0). c) Neutron tomogram slice from a TKR patient (same sample as in a), showing matrix damage as areas of lower attenuation (red arrow).

This degeneration shows a clear progression that can be matched to histological images and histopathological grading of the cartilage (Figure 5.5). At grade 0, both images show a smooth cartilage surface and consistent cell distribution. Grade 2 samples show beginning fibrillation in the superficial zone, which then progresses into deep cracks and a completely disrupted surface at higher grades (Figure 5.5).

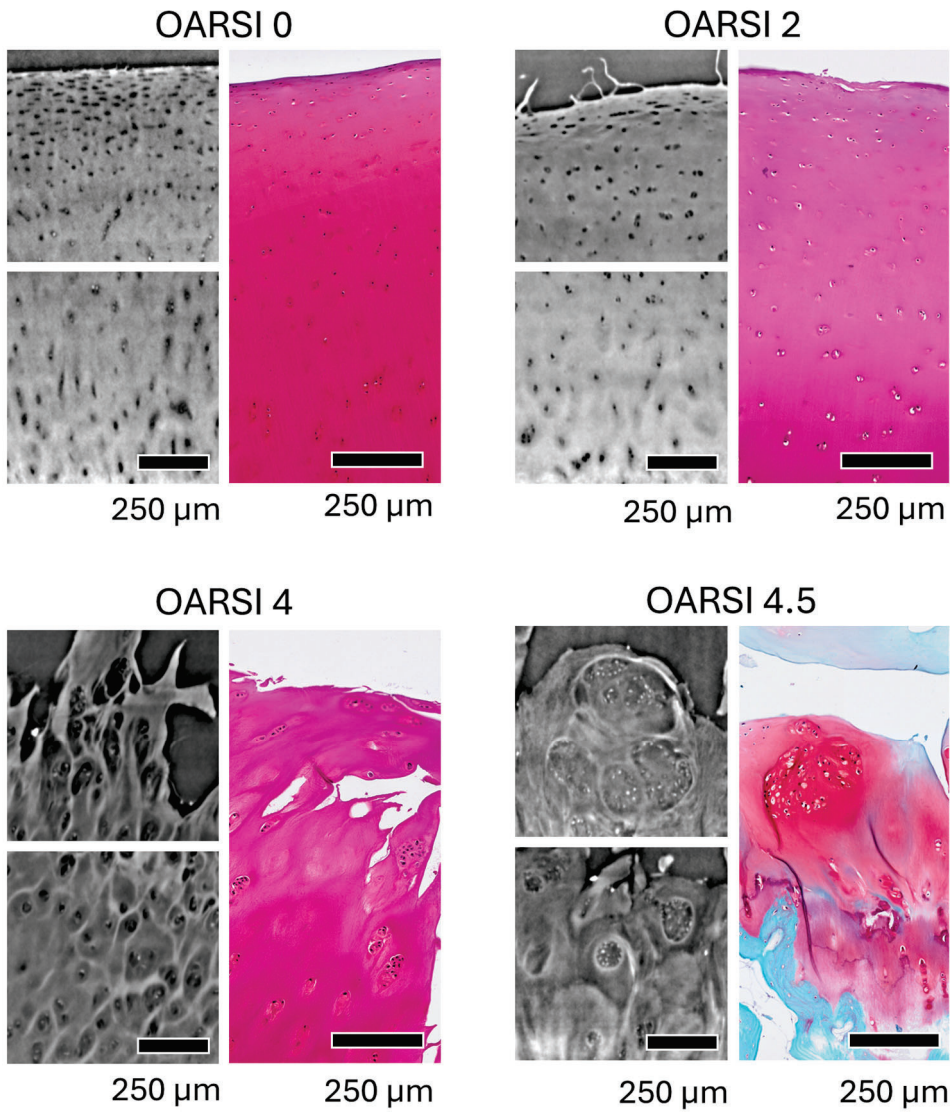

Figure 5.5: Degeneration progression. Phase-contrast tomogram slices taken near the surface (top left) and near the bone (bottom left) are shown alongside Safranin-O histology (right). Samples come from four donors at different stages of degeneration, ranging from healthy cartilage (OARSI 0) to severe degeneration (OARSI 4.5).

Cell changes such as clustering are also clearly visible in both phase-contrast tomograms and histology images.

Quantification of depth-wise profiles of chondrocyte properties (Study I) and matrix hydrogen density (Study II) also reveal degenerative and age-related changes. Notably, these properties show consistent distinct profile shapes in healthy samples before becoming increasingly erratic with increasing age or degeneration (Figure 5.6a). Differences in matrix hydrogen density in the form of neutron attenuation are more closely related to cartilage thickness than differences in chondrocyte properties.

The chondrocyte property profiles show more distinct relationships to OARSI grade. Healthy samples generally have distinct profile shapes, showing a shift in cell angle from the surface to the depths of the tissue (Figure 5.6b) as well as spikes in cell density in the superficial and deep zones (Figure 5.6.c). These shapes are lost with increasing degeneration, producing flatter profiles.

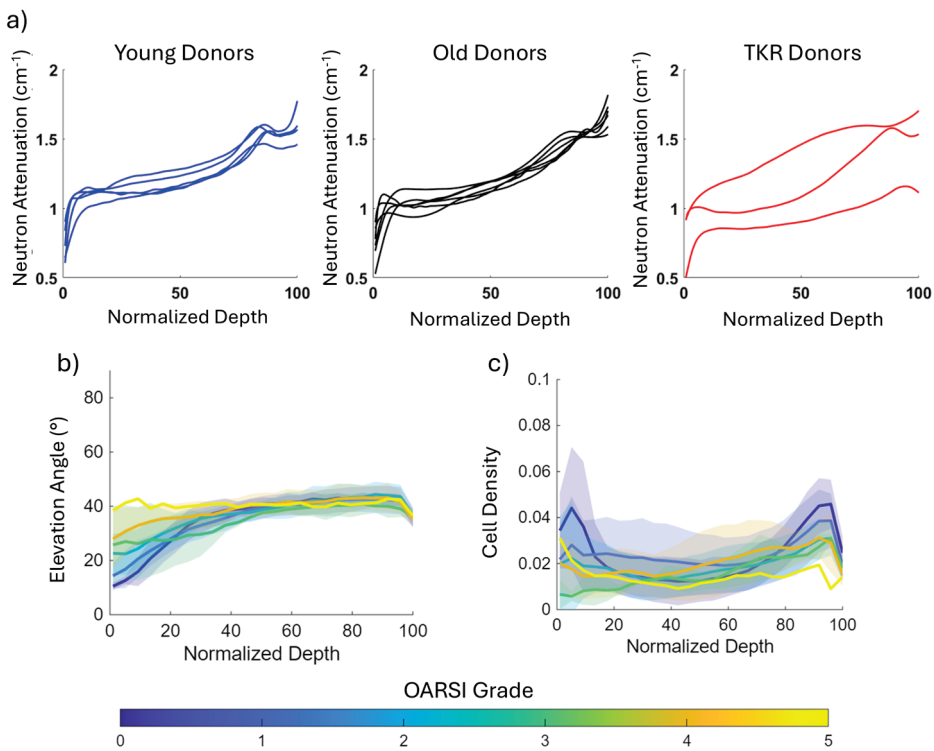

Figure 5.6: Quantification of Degenerative Changes. a) Neutron attenuation profiles from cartilage surface to bone interface, separated by young (< 45 y) and old (> 60 y) donors without known knee OA and TKR patients in Study II. b) Average cell elevation angle profile averaged by OARSI grade in Study I. c) Average cell density profile averaged by OARSI grade in Study I.

Particularly in the superficial layer, chondrocyte properties can be tied to degeneration via statistical analysis. This analysis shows that the angle between the cells and the tissue surface increases by an average of 3.9° (95% CI 2.9-4.9) per OARSI grade (5) unit as the flattened organization in the superficial layer is lost.

5.4 Tissue water dynamics (Study III-IV)

D_2O concentrations calculated from the raw water diffusion visualization gives a clear image of the dynamic process of water exchange (Figure 5.7a), including an edge effect causing some inhomogeneity. Water concentration increases rapidly along the surface as well as the sides of the cartilage, and more slowly in the center. Quantification of this sequence shows the progression of the diffusion process itself (Figure 5.7b-c). Profiles of concentration over depth show a decrease with depth at first, before approaching uniform concentration. Over time, similar diffusive curves are present at different depths, with the concentration increasing more slowly deeper in the tissue. Diffusion-tensor MRI produces diffusion coefficients that decrease

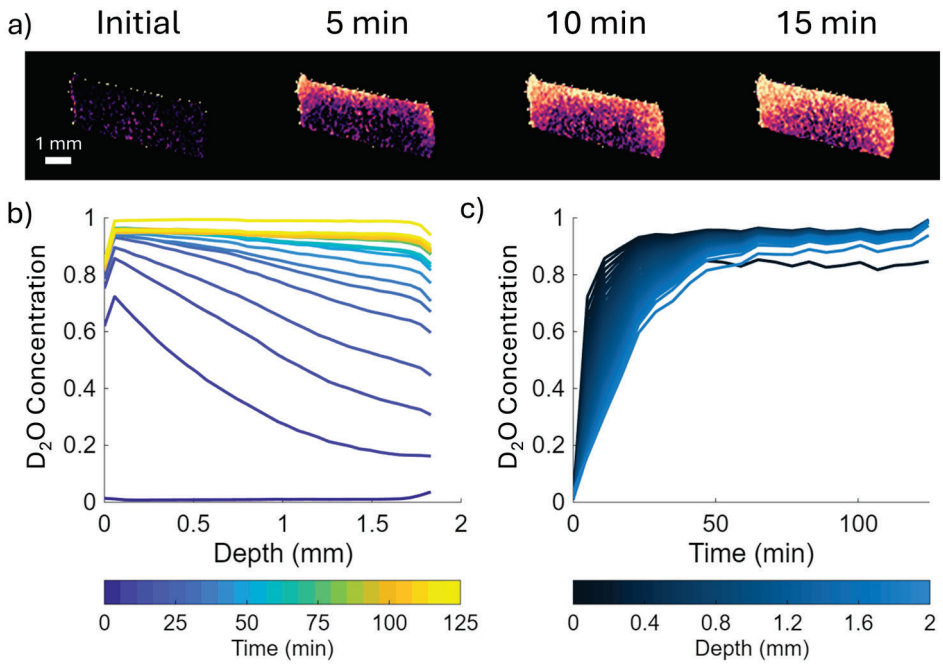

Figure 5.7: Macroscopic Water Diffusion. a) Progression of D2O diffusion into bovine articular cartilage, with brighter color indicating higher D2O concentration. b) Profiles of D2O concentration over depth at different times in the same cartilage sample. c) Profiles of D2O concentration over time at different depths.

with depth through the superficial and intermediate zones while being constant in the deep zone in cartilage, and which vary around an average value in meniscus (Figure 5.8). Finite element modelling of these coefficients in articular cartilage based on the neutron data produce values that are in agreement with deep zone diffusion coefficients measured by MRI when adjusted for the difference between H_2O and D_2O (112), but in the best fits are constant throughout the tissue. In meniscus, finite element modelling produced poor fits for diffusion coefficients.

Broad QENS measurements reveal the dynamics of the water within bovine articular cartilage, showing a clear signal for long-range diffusion (Figure 5.9a). Fitting allows

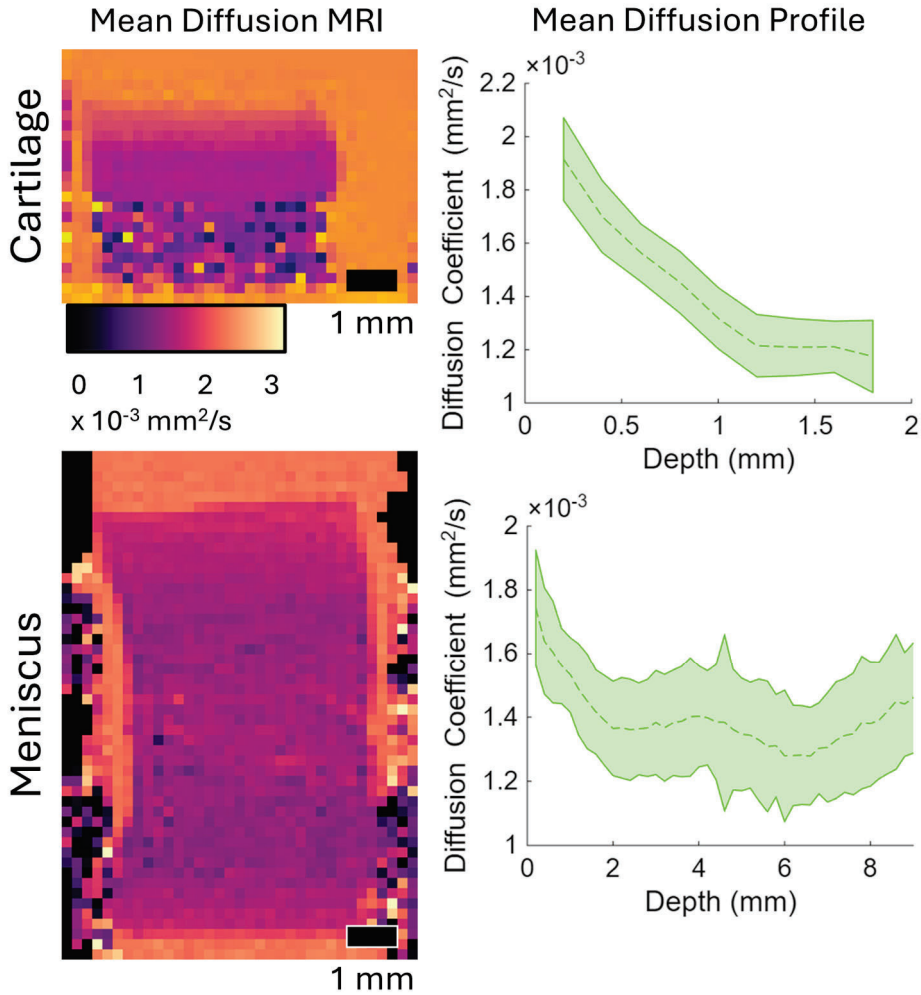

Figure 5.8: Diffusion MRI. Mean diffusion maps of cartilage (top) and meniscus (bottom) alongside profiles of the average diffusion coefficient at different depths from the top tissue surface.

diffusion coefficients for bulk water to be calculated to 3.16 x 10^{-3} mm^2/s in the intermediate zone and 3.86 x 10^{-3} mm^2/s in the deep zone (Figure 5.9b). A second Lorentzian corresponds to some higher-energy molecular movement likely resulting from confined water and contributions from rotational motions.

Narrow QENS reveals a weak quasielastic signal only visible in Q-summed spectra and in the inelastic fixed-window scan. Measurements are dominated by the bulk water signal appearing as a flat background on scans at this energy range.

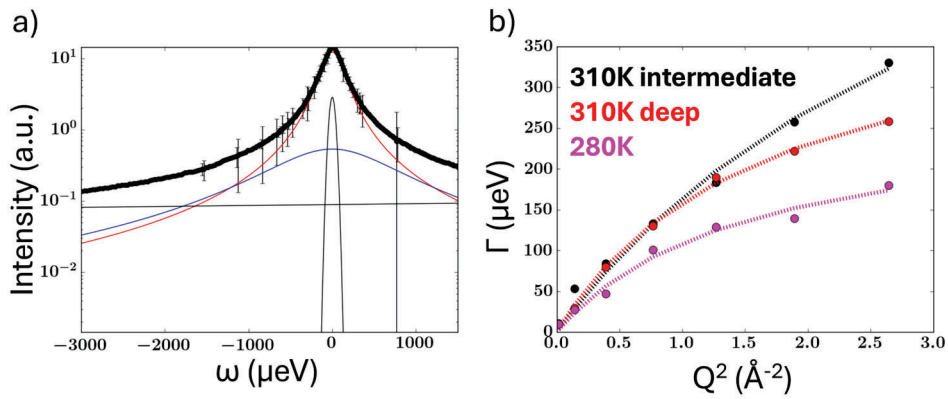

Figure 5.9: QENS. a) Example of fitting. Shown is a quasielastic spetra at Q = 0.875 $Å^{-1}$ alongside a fitted broad and narrow Lorentzian. b) Q2-dependency of the narrow Lorentzian in broad QENS measurements of articular cartilage, corresponding to bulk water diffusion alongside the fitted water diffusion model.

6 Discussion

6.1 General

The aim of this thesis was to investigate the ability of neutron and synchrotron techniques to characterize soft knee tissues in novel ways. Studies I-III focused on different approaches to conventional tomographic imaging, all in an effort to characterize different aspects of the tissues. Phase-contrast tomography was used in Study I to visualize chondrocytes as well as matrix damage in tissue by visualizing transitions between materials. Study II shifted the focus to the overall cartilage tissue matrix with neturon tomography to visualize hydrogen density, which then extended into visualization of diffusive water exchange through D_2O application in Study III. Insights into this water exchange were then complemented through direct investigations of water dynamics via QENS in Study IV.

These technques were explored due to their ability to probe various metrics of interest, i.e. tissue integrity, chondrocyte distribution, matrix protein density, and tissue water dynamics. All of these metrics are vital to the healthy functioning of the tissue, and consequently potential vectors for degenerative processes. A particular focus of the thesis was developing these techquies as tools for further application within the field. This could in turn lead to a better understanding of both the baseline state of the tissue and alterations therein, which might be indicative of osteoarthritis-related degeneration.

The techniques presented within the thesis can be seen as extensions to existing tools, such as synchrotron phase-contrast imaging producing histology-quality images of soft tissues in three dimensions, or neutron imaging expanding on the ability to detect water content or diffusion via MRI. They also provide additional novel applications in the field of soft knee tissues, such as the ability to visualize diffusion directly with neutron imaging, or probe nanosecond-scale motions with

QENS. Novel techniques are not without their challenges, however, particularly when it comes to the accessiblity of large facilities and validation against existing ground truths. Both the highlighted benefits and challenges of these techniques will be discussed in the following sections.

6.2 Tissue specific information revealed by the techniques

All three techniques were novel in their application to soft knee tissues. Phase-contrast imaging is the most established, having been previously used for cartilage and meniscus research (9-11) but not applied to larger datasets from human donors with a wide range of tissue degeneration levels. Neutron imaging, in contrast, had not previously been applied to soft knee tissues at all, and outside of some pilot images (12) the field lacks previous work on animal soft tissue in general, with the closest analogues to this work having been performed on bone (17, 18, 70) and plant tissues (14, 15). Quasi-elastic scattering similarly has not been performed on musculoskeletal tissues before, with the closest analogues being a study on brain tissue (22) as well as studies on glycosaminoglycan-based hydrogels (113, 114). Consequently, this section discusses the general information revealed by the techniques in articular cartilage with subsequent sections examining the applications to tissue degeneration and water dynamics, and potential future developments needed for the techniques to reach their full potential in the field.

6.2.1 Phase-contrast imaging

Phase-contrast imaging in Study I enabled both qualitative visualizations and quantitative metrics of chondrocyte properties and general tissue integrity in articular cartilage. Chondrocytes are clearly visible, captured in 3D, and retain a shape unaffected by chemical fixation in contrast to histology. Fully automatic segmentation, while introducing some limitations in which bodies could be distinguished, allowed for the study of substantially larger volumes of cartilage than examined in comparable work on chondrocyte tomography (50). Segmentation could be improved with increased resolution, as demonstrated by the higher-resolution ForMAX images, although this would come at the cost of smaller volumes imaged. Previous phase-contrast work on cartilage similarly performed chondrocyte segmentation using even-higher resolution images (10) but does not report segmentation in comparable resolution images. In directly comparable experiments on bovine cartilage better segmentation was possible (11) in part due to the larger size of bovine chondrocytes.

Quantification allowed for an additional angle of study for chondrocyte properties in addition to the visualizations. Profiles of properties like chondrocyte cluster angle or shape clearly correspond to the zonal divisions within the cartilage. While these

quantifications are possible to perform in histology as well, they reveal far less information and are much more prone to sampling bias resulting from intra-sample variance. Consequently, quantification of phase-contrast volumes can be seen as a previously unavailable tool for gauging the health status of cartilage.

6.2.2 Neutron imaging

Neutron imaging has a number of potential applications through the visualization of the density of the cartilage matrix resulting from the ability to use heavy water for contrast. With hydrogen dominating the neutron attenuation in tissue, and heavy water having a factor seven lower attenuation than regular water, heavy water treatment effectively renders the water contribution to the signal negligible compared to that of hydrogen bound into proteins or fatty tissues. Cartilage tissue hydrated with regular water shows no change with depth in neutron attenuation, suggesting a uniform concentration of hydrogen when both are present. Tissue hydrated with heavy water instead shows attenuation increasing with depth, consistent with a higher collagen density in the deeper zones of cartilage (115). Consequently, tomography of heavy water-treated tissue could produce a map of relative protein density in 3D, potentially with fewer confounding factors than corresponding MRI techniques (6) as the sensitivity of neutron imaging to the magnetic properties of hydrogen in biological tissue is negligible.

While neutron imaging lacks the resolution or contrast to detect chondrocytes or collagen fibril structures, it does produce higher resolution than most MRI approaches at comparable imaging times. Resolution could potentially be pushed into the sub-10 μm realm where such details could theoretically be resolved with neutrons (116) but the contrast would likely be insufficient to resolve such details. Additionally, imaging times on the order of 50 hours would be required, posing substantial challenges when imaging biological tissue. Such an image was attempted as part of this thesis, pushing voxel size to ~2.5 μm at the ICON neutron microscope (72), but the resulting data was unusable due to movement artifacts and consequently not included in publication. The next generation of sources might reduce imaging times enough to make higher resolutions feasible, however, with the design specifications for the ODIN beamline at ESS listing a neutron flux at the sample position about ~5 times higher than the current highest-flux imaging beamline NeXT (71, 117). With MRI (118) such resolutions are also achievable, albeit with even longer imaging times (exceeding 50 hours). The resolutions produced with current neutron imaging approaches are also perfectly sufficient for the study of general protein or water density, which remains the primary motivation to use neutron imaging over an X-ray technique.

6.2.3 Quasi-elastic neutron scattering

QENS was able to characterize rotational and translational water motions within articular cartilage, although the resulting signal is mingled with one resulting from cartilage components. Temperature dependencies show the presence of some level of dynamics not dependent on liquid water as a quasielastic signal is still present at 250K but subsides at lower temperatures, which could potentially have implications for tissue storage as 250K is below the temperature of conventional freezers. No low-energy water dynamics were observed, indicating that a different approach using D_2O for contrast in a similar manner as applied to isolated protein solutions (21) would be preferrable for future studies of low energy cartilage dynamics.

6.2.4 Limitations

A primary limitation with all three techniques is the requirement of large facilities with limited beamtime and competitive application procedures. Phase-contrast imaging is in principle also possible to perform using laboratory X-ray sources (80, 119) but this comes at the cost of drastically increased imaging times, which could complicate experiments. Neutron imaging and quasi-elastic scattering are completely limited to large-scale facilities, with relatively long measuring times at even the most powerful sources. Currently these are quite limited in number, with only ILL and SINQ providing the flux for comparable experiments in Europe, although the upcoming completion of the ESS will significantly increase available high flux beamtime. Synchrotron beamlines, while still limited, are substantially more in number, and newer-generation sources such as MAX IV can potentially reduce the trade-off between resolution and imaged volume through increased power, although radiation damage potentially becomes an issue.

Furthermore, while these techniques are powerful for *ex vivo* research, they are excluded from most *in vivo* approaches. Synchrotron imaging can be performed on live animals (120) but the high radiation doses involved raise ethical questions in animal experiments and completely exclude use on human subjects. Consequently, only very few beamlines such as the Imaging and Medical Beamline in Australia (121) allow for *in vivo* imaging. Neutron imaging likewise is unsuitable for *in vivo* use due to radiation dose and the possibility of induced radioactivity. Additionally, the low imaging times and high neutron attenuation in hydrogen rich materials means that neutron imaging requires immobile samples of <10 mm thickness, further reducing its suitability for in-vivo research. QENS faces even stricter sample restrictions, with sample thicknesses of ~100 μm required to maximize quasi-elastic signal while minimizing noise due to multiple scattering.

6.3 Studying articular cartilage degeneration

The details revealed by both imaging techniques provide novel angles for the study of the progression of OA-related degeneration in cartilage.

6.3.1 Virtual histology

Phase-contrast images visually capture features of degeneration both in chondrocyte distribution as well as in the matrix itself, in a manner comparable to or even exceeding the quality of histological imaging. Notably, as the phase-contrast images are taken of unfixed tissue immersed in PBS makes surface damage more visible than in dehydrated tissue flattened onto a microscope slide. The approach also reduces the variability inherent to sectioning by imaging a larger volume of tissue. The high image quality opens up the possibility of developing a grading system comparable to the OARSI scale (5) for phase-contrast images, especially as similar work has been performed using chemical contrast enhancement (49). As phase-contrast imaging avoids chemical manipulation of samples, it also enables complementary experiments, making it ideal for studies where it is vital that both general degeneration evaluation and another characterization technique be performed on the same tissue.

6.3.2 Chondrocyte quantification

Quantification of chondrocytes showed clear trends when compared to the qualitative measure derived from the OARSI scale. Quantified cell density as well as chondrocyte cluster orientation and aspect ratio all show characteristic profiles in healthy samples which flatten at higher OARSI grades, likely as the result of a breakdown of zonal divisions in the tissue. Statistical analyses further reinforce this, particularly through showing altered chondrocyte orientations in the surface layer at higher levels of degeneration. This can be compared to previous work primarily studying chondrocyte enlargement as a marker of early OA (122-124), something feasibly achievable with increased resolution in phase-contrast imaging. This increased resolution is achievable with current methods, albeit at the trade-off of a smaller imaging volume. Such improvements, together with increased study of chondrocyte orientation and clustering, could both provide increased insight into early OA and potentially be a component of an improved system of cartilage degeneration evaluation.

6.3.3 Hydrogen density

Hydrogen density as evaluated by neutron tomography of D_2O-treated samples can be seen as a proxy for the density of the cartilage matrix, i.e. the ratio of protein to water. This density in turn shows characteristic profiles with the depth in the tissue which are disrupted by degeneration much like the chondrocyte property profiles, indicating a breakdown of zonal divisions. While more detailed conclusions about the link in hydrogen density and degeneration may be possible with larger sample sizes imaged, the ability of neutron imaging to study water flow through D_2O exchange (14, 15, 18) is likely to be more valuable to the study of degeneration as healthy cartilage relies on fluid pressure to support load.

6.3.4 Limitations

Compared to traditional histology, the main limitation of phase-contrast based virtual histology is the inability to detect non-morphological signs of degeneration such as proteoglycan depletion. While stain-equivalent results can be obtained using X-ray contrast agents (125) such an approach in turn limits the ability for sample re-use that otherwise is a core benefit of phase-contrast. For quantitative degeneration evaluation, the main limitation is the difficulties in chondrocyte segmentation resulting from image quality variations and limited resolution. Evaluation of the matrix density via neutron imaging is in turn limited by difficulties in disentangling contributions of different protein components as well as by the need for a 3D method of characterizing cartilage density to calibrate measures of the protein component.

6.4 Exploring water dynamics

Both neutron imaging and quasi-elastic neutron scattering give insight into the water dynamics of articular cartilage and meniscus, on different length and time scales.

6.4.1 Visualizing diffusion

Neutron tomography clearly visualizes 3D water diffusion in both articular cartilage and meniscus in real time, bringing into the realm of soft tissue research something previously only demonstrated in plants (14, 15). It also provides a more direct investigation of water exchange than previous work limited to studying the before and after of H_2O-D_2O exchange (18). Additionally, unlike previous work using contrast agents and X-ray techniques to visualize the diffusion of larger molecules (126-128), this technique accesses water diffusion directly. As cartilage degeneration disrupts the collagen network and depletes proteoglycans (5, 32), water permeability

and thus diffusion will increase with increasing levels of degeneration. Consequently, diffusion visualization could be applied to the study of OA-related degeneration by studying changes in tissue water diffusion. Furthermore, these changes could reveal the effects other degeneration-related changes such as pathologic vascularization (129, 130). The diffusion visualization potentially also reveals the presence of mechanisms inhibiting long-range diffusion that are not present at the shorter ranges probed by diffusion MRI, as the thicker meniscus did not reach D_2O saturation in the expected time.

6.4.2 Modelling diffusion

Modelling diffusion based on Fick's law revealed diffusion coefficients that were consistent with MRI-derived values in overall diffusivity, but not in depth-dependency. Particularly in the superficial zone of cartilage, the model indicates slower diffusion than what would be predicted by MRI, potentially indicating some mechanism inhibiting diffusion on longer length scales than the μm range probed by diffusion MRI. However, this is complicated by the geometry of the sample as the area of liquid contact at the top is smaller than the full top area of the sample.

QENS allowed for fitting of diffusion coefficients and residence times according to a jump diffusion model (111), resulting in a view of dynamics on a much shorter timescale than MRI. Diffusion coefficients are a factor 2-3 larger than those measured by MRI, but are similar if a bit higher than corresponding values reported in hydrogels (113, 114) or brain tissue (22). This indicates that restrictions on the diffusion of water in cartilage arise on the micrometer-microsecond scale and are not present on the scales probed by QENS. Also visible is a difference in residence time between the intermediate and deep layers of cartilage, which may be a result of water-proteoglycan interactions increasing the time between diffusive jumps, but confirming this result would require a larger sample size.

6.4.3 Limitations

Diffusion studies using neutron images are primarily limited by resolution trade-offs and by calibration. Resolution at a given neutron flux and experimental station quality is fundamentally a trade-off between temporal and spatial priorities. However, resolutions are still higher than DTI on comparable experiment timescales, with matching DTI requiring 48+ hours (131). Calibration could also be improved by imaging samples soaked in an excess of water with different known H_2O-D_2O ratios, although such experiments would require substantial non-imaging treatment time on each sample, which poses logistical difficulties with the timeframes involved at large-scale facilities.

The QENS studies of articular cartilage were primarily limited by a low sample size resulting from limitations on beamtime and difficulties in sample preparation. QENS requires large ~100 μm thick slices of cartilage cut parallel to the tissue surface, which is difficult on non-flat condyles. The cutting technique also does not match standard slicing protocols for histology, which would cut thinner slices perpendicular to the surface (37). Consequently, conclusions could be significantly reinforced by extending the pilot experiment presented herein with a more targeted water diffusion experiment with a larger sample size.

6.5 Future perspectives

There are a number of potential future avenues for research using these techniques. The baseline experiments presented in this work could be improved through both methods development such as improved sample preparation for QENS as well as through the future availaibility of more powerful facilities, like the higher flux offered by ESS instruments (117). Several of them could potentially be performed in-situ with mechanical loading, giving insight into how the characterized tissue properties relate to mechanical performance of the tissue.

6.5.1 Near-term: Immediate applications

As the techniques presented are highly compatible with complementary or in-situ experiments, the immediate avenues for further research involve applications of simultaneous mechanical loading. In the case of phase-contrast imaging of cartilage, adjacent data to that presented in the thesis was already obtained by our experimental team to evaluate soft knee tissue mechanics. Particularly the potential for tracking chondrocyte and meniscal fibre displacement under load (11) and the effect of cartilage shape on mechanical properties (132) has been demonstrated in bovine cartilage tissue, and work extending this to a larger sample set of human donors is ongoing.

Neutron techniques could similarly be applied to understand tissue behaviour under load. D_2O-treated tissue would allow evaluation of the compressibility of the protein component of the tissue through the visualization of altered hydrogen density before and after loading. An at the time of writing unpublished set of pilot neutron tomograms of mechanically compressed cartilage and meniscus were acquired adjacent to the work performed in this thesis, demonstrating that expelled water could be quantified although results on protein compressibility were inconclusive. Likewise, diffusion imaging could be combined with loading in order to quantify load effects on diffusivity or water motion. QENS could also be combined with loading to detect alterations in both water and protein dynamics under pressure, something previously demonstrated on silk fibres (23). The primary challenges

needing to be resolved for a similar experiment in cartilage would be the development of a loading device compatible with neutron spectrometers as well as gaining an improved enough understanding of the baseline dynamics to evaluate load-related changes.

Outside of load responses, these techniques offer novel ways to examine degeneration. Phase-contrast images could be extended into a proper grading system in a manner similar to that demonstrated on contrast-enhanced absorption X-ray images (49), which could combine with quantitative measures to produce a more detailed measure of degeneration level than previous standards. Diffusion studies both using imaging and QENS could also be applied to degenerated tissues, evaluating to how macroscopic and nanosecond scale diffusion change with degeneration, and whether this differs from known microsecond-scale diffusion changes studied with MRI (35, 36). Here the primary challenge would be measuring large enough sample sets to separate degeneration effects from natural biological variability, as both diffusion imaging and QENS experiments would require a minimum of 2-3 hours of measurement time per sample. QENS also poses the additional challenge of requiring a relatively large amount of tissue per measurement (ideally covering a 3x4 cm area), limiting use on scarce human tissue.

6.5.2 Long-term: Expanded future usage

After more extensive follow-up work, the techniques piloted here could open up a number of powerful future approaches for the study of both soft knee tissues as well as soft tissue in general. Phase-contrast imaging of cartilage, especially if a grading method similar to that proposed for chemically contrast enhanced images (49) is developed, could supplement traditional histology for degeneration assessment. Similar advances have already been made in other biomedical fields, e.g. in the use of phase-contrast to supplement histology in cancer diagnosis (133, 134) and surgical biopsy assessment (135). Furthermore, the ability to quantify chondrocyte properties in such images could allow for more detailed degeneration assessment less dependent on the judgement of human pathologists. If lab-source approaches similar to those used in cancer diagnostics were developed, this could then potentially allow for very large sample sizes if it could be performed as routine imaging following e.g. total knee replacement surgery. Such large datasets could produce much more extensive links between the details of the physical degeneration of the cartilage tissue and the symptoms experienced by individual patients.

Combining phase-contrast with neutron imaging and scattering could then extend this from degeneration assessment into a more detailed understanding of tissue composition and properties, with applications both for understanding and modelling load response. Tracking of chondrocytes or other tissue features during loading could produce more detailed strain mapping of the tissue (11, 132), providing vital

data for more extensive load modelling. Neutron imaging could potentially also be adapted to characterize the water permeability of both cartilage or meniscus by imaging as water is expelled by applied load and calculating water movement rates. As hydraulic permeability is an important metric in the mechanical properties of these tissues (136, 137), more accurately assessing it could improve mechanical models of the tissue. Furthermore, both techniques could be utilized for the characterization of bioengineered tissue-like materials in order to tune their properties to replicate the characteristics of existing soft knee tissues.

Finally, neutron-based characterization of water dynamics could be applied to the study of other tissues beyond the knee. QENS has already been applied to the study of neural water dynamics (22) in addition to the current work on cartilage and could feasibly expand to several others. Imaging of diffusive flow with neutrons could likewise be applied to other tissues where longer-range diffusive motions are of interest. The brain is an obvious candidate, as currently diffusion MRI is widely applied in neural studies (22, 131, 138), but it could also be feasible to adapt methods previously used in plants (14, 15) to study fluid transport through blood vessel networks or similar transport channels.

7 Summary and conclusions

The overall aim of this thesis was to develop and explore novel synchrotron- and neutron-based techniques for characterizing soft knee tissues in relation to their health status as well as water-diffusive properties relevant to tissue function. Synchrotron phase-contrast and neutron tomography provided new structural information about the tissue, with initial neutron images opening the possibility for dynamic studies of water flow. Alongside traditional histology and MRI approaches, these tomographic techniques were complemented by another novel neutron approach in the form of QENS, demonstrating a number of new possible angles of study for soft knee tissue biology and bioengineering.

Below, the main conclusions of each study (I-IV) are summarized.

I. *Phase-contrast synchrotron imaging provides histology-quality images in full 3D, and allow for more extensive quantitative analysis.* Imaging a large set of human samples both revealed clearly visible qualitative markers of tissue degeneration as well as providing quantitative metrics for chondrocyte distribution. Additionally, variability is reduced compared to traditional histology due to the ability to image larger volumes, and the technique preserves the tissue for later complementary experiments.

II. *Neutron tomography provides attenuation matching tissue hydrogen density and consequently water content when correctly treated.* Samples treated with heavy water show the density of the hydrogen in the protein matrix, complementing X-ray and MRI-based images. Degenerative effects were less clearly visible, but the ability to visualize water content provides the tools for the study of water dynamics.

III. *Neutron tomography can directly vizualize water diffusion in articular cartilage and meniscus in real time*. The progression of diffusion through the tissue with time during the exchange of H_2O for D_2O is clearly visible, both visually in images and in plotted profiles. Relative concentrations can be computed using reference volumes, allowing for estimation of diffusion coefficents that agree well with MRI.

IV. *Quasi-elastic neutron scattering reveals the complexity and timescales of cartilage water dynamics*. Fitting of data reveals both fast confined motions and slower long-range jump diffusion motions. Jump diffusion cannot be separated into multiple processes, indicating that the effect of the cartilage protein matrix on water diffusion occurs only on longer timescales. Low-energy motions are restricted to the protein matrix, as no low-energy water motions could be discerned. Consequently, QENS is best suited to studies of cartilage protein motion changes in a D_2O environment.

References

1. Hunter DJ, Bierma-Zeinstra S. Osteoarthritis. *The Lancet*. 2019;**393**(10182):1745-59. doi: 10.1016/S0140-6736(19)30417-9

2. Steinmetz JD, Culbreth GT, Haile LM, Rafferty Q, Lo J, Fukutaki KG, et al. Global, regional, and national burden of osteoarthritis, 1990-2020 and projections to 2050: a systematic analysis for the Global Burden of Disease Study 2021. *The Lancet Rheumatology*. 2023;**5**(9):e508-e22. doi: 10.1016/S2665-9913(23)00163-7

3. Turkiewicz A, Petersson IF, Björk J, Hawker G, Dahlberg LE, Lohmander LS, et al. Current and future impact of osteoarthritis on health care: a population-based study with projections to year 2032. *Osteoarthritis Cartilage*. 2014;**22**(11):1826-32. doi: 10.1016/j.joca.2014.07.015

4. Kloppenburg M, Namane M, Cicuttini F. Osteoarthritis. *The Lancet*. 2025;**405**(10472):71-85. doi: 10.1016/S0140-6736(24)02322-5

5. Pritzker KPH, Gay S, Jimenez SA, Ostergaard K, Pelletier JP, Revell PA, et al. Osteoarthritis cartilage histopathology: grading and staging. *Osteoarthritis and Cartilage*. 2006;**14**(1):13-29. doi: 10.1016/j.joca.2005.07.014

6. Emanuel KS, Kellner LJ, Peters MJM, Haartmans MJJ, Hooijmans MT, Emans PJ. The relation between the biochemical composition of knee articular cartilage and quantitative MRI: a systematic review and meta-analysis. *Osteoarthritis and Cartilage*. 2022;**30**(5):650-62. doi: 10.1016/j.joca.2021.10.016

7. Sophia Fox AJ, Bedi A, Rodeo SA. The Basic Science of Articular Cartilage: Structure, Composition, and Function. *Sports Health*. 2009;**1**(6):461-8. doi: doi.org/10.1177/1941738109350438

8. Saccomano M, Albers J, Tromba G, Dobrivojevic Radmilovic M, Gajovic S, Alves F, et al. Synchrotron inline phase contrast microCT enables detailed virtual histology of embedded soft-tissue samples with and without staining. *Journal of Synchrotron Radiation*. 2018;**25**(4):1153-61. doi: 10.1107/S1600577518005489

9. Einarsson E, Pierantoni M, Novak V, Svensson J, Isaksson H, Englund M. Phase-contrast enhanced synchrotron micro-tomography of human meniscus tissue. *Osteoarthritis and Cartilage*. 2022;**30**(9):1222-33. doi: 10.1016/j.joca.2022.06.003

10. Horng A, Stroebel J, Geith T, Milz S, Pacureanu A, Yang Y, et al. Multiscale X-ray phase contrast imaging of human cartilage for investigating osteoarthritis formation. *Journal of Biomedical Science*. 2021;**28**(1):42. doi: 10.1186/s12929-021-00739-1

11. Dejea H, Pierantoni M, Orozco GA, B. Wrammerfors ET, Gstöhl SJ, Schlepütz CM, et al. In Situ Loading and Time-Resolved Synchrotron-Based Phase Contrast Tomography for the Mechanical Investigation of Connective Knee Tissues: A Proof-of-Concept Study. *Advanced Science*. 2024;**11**(21):2308811. doi: 10.1002/advs.202308811

12. Bilheux HZ, Cekanova M, Warren JM, Meagher MJ, Ross RD, Bilheux JC, et al. Neutron Radiography and Computed Tomography of Biological Systems at the Oak Ridge National Laboratory's High Flux Isotope Reactor. *JoVE*. 2021(171):e61688. doi: 10.3791/61688

13. Hassanein RK. Correction methods for the quantitative evaluation of thermal neutron tomography: ETH Zurich; 2006.

14. Defraeye T, Derome D, Aregawi W, Cantré D, Hartmann S, Lehmann E, et al. Quantitative neutron imaging of water distribution, venation network and sap flow in leaves. *Planta*. 2014;**240**(2):423-36. doi: 10.1007/s00425-014-2093-3

15. Tötzke C, Kardjilov N, Manke I, Oswald SE. Capturing 3D Water Flow in Rooted Soil by Ultra-fast Neutron Tomography. *Scientific Reports*. 2017;**7**(1):6192. doi: 10.1038/s41598-017-06046-w

16. Tötzke C, Kardjilov N, Lenoir N, Manke I, Oswald SE, Tengattini A. What comes NeXT? – High-Speed Neutron Tomography at ILL. *Opt Express*. 2019;**27**(20):28640-8. doi: 10.1364/OE.27.028640

17. Törnquist E, Le Cann S, Tengattini A, Helfen L, Kok J, Hall SA, et al. The Hydration State of Bone Tissue Affects Contrast in Neutron Tomographic Images. *Frontiers in Bioengineering and Biotechnology*. 2022;**10**. doi: 10.3389/fbioe.2022.911866

18. Silveira A, Kardjilov N, Markötter H, Longo E, Greving I, Lasch P, et al. Water flow through bone: Neutron tomography reveals differences in water permeability between osteocytic and anosteocytic bone material. *Materials & Design*. 2022;**224**:111275. doi: 10.1016/j.matdes.2022.111275

19. Bée M. Quasielastic Neutron Scattering, Principles and Applications in Solid State Chemistry, Biology and Materials Science: Taylor & Francis; 1988.

20. Qvist J, Schober H, Halle B. Structural dynamics of supercooled water from quasielastic neutron scattering and molecular simulations. *The Journal of Chemical Physics*. 2011;**134**(14). doi: 10.1063/1.3578472

21. Grimaldo M, Roosen-Runge F, Jalarvo N, Zamponi M, Zanini F, Hennig M, et al. High-resolution neutron spectroscopy on protein solution samples. *EPJ Web of Conferences*. 2015;**83**:02005. doi: 10.1051/epjconf/20158302005

22. Natali F, Dolce C, Peters J, Stelletta C, Demé B, Ollivier J, et al. Anomalous water dynamics in brain: a combined diffusion magnetic resonance imaging and neutron scattering investigation. *Journal of The Royal Society Interface*. 2019;**16**(157):20190186. doi: 10.1098/rsif.2019.0186

23. Krasnov I, Seydel T, Greving I, Blankenburg M, Vollrath F, Müller M. Strain-dependent fractional molecular diffusion in humid spider silk fibres. *Journal of The Royal Society Interface*. 2016;**13**(122):20160506. doi: 10.1098/rsif.2016.0506

24. Martensson N, Eriksson M. The saga of MAX IV, the first multi-bend achromat synchrotron light source. *Nuclear Instruments and Methods in Physics Research Section A: Accelerators, Spectrometers, Detectors and Associated Equipment*. 2018;**907**:97-104. doi: 10.1016/j.nima.2018.03.018

25. Garoby R, Vergara A, Danared H, Alonso I, Bargallo E, Cheymol B, et al. The European Spallation Source Design. *Physica Scripta*. 2018;**93**(1):014001. doi: 10.1088/1402-4896/aa9bff

26. Nygard K, McDonald SA, Gonzalez JB, Haghighat V, Appel C, Larsson E, et al. ForMAX - a beamline for multiscale and multimodal structural characterization of hierarchical materials. *Journal of Synchrotron Radiation*. 2024;**31**(2):363-77. doi: 10.1107/S1600577524001048

27. Matěj Z, Mokso R, Larsson K, Hardion V, Spruce D. The MAX IV imaging concept. *Advanced Structural and Chemical Imaging*. 2016;**2**(1):16. doi: 10.1186/s40679-016-0029-7

28. Strobl M. The Scope of the Imaging Instrument Project ODIN at ESS. *Physics Procedia*. 2015;**69**:18-26. doi: 10.1016/j.phpro.2015.07.002

29. Hirschmann MT, Müller W. Complex function of the knee joint: the current understanding of the knee. *Knee Surgery, Sports Traumatology, Arthroscopy*. 2015;**23**(10):2780-8. doi: 10.1007/s00167-015-3619-3

30. Kuczyński N, Boś J, Białoskórska K, Aleksandrowicz Z, Turoń B, Zabrzyńska M, et al. The Meniscus: Basic Science and Therapeutic Approaches. *Journal of Clinical Medicine*. 2025;**14**(6):2020. doi: 10.3390/jcm14062020

31. Oliveira I, Gonçalves C, Reis RL, Oliveira JM. Synovial Knee Joint. In: Oliveira JM, Reis RL, editors. Regenerative Strategies for the Treatment of Knee Joint Disabilities. Cham: Springer International Publishing; 2017. p. 21-8.

32. Buckwalter JA, Mankin HJ, Grodzinsky AJ. Articular cartilage and osteoarthritis. *Instructional course lectures*. 2005;**54**:465-80.

33. Baron SL, Jazrawi LM. Anatomy and Function. In: Strauss EJ, Jazrawi LM, editors. The Management of Meniscal Pathology: From Meniscectomy to Repair and Transplantation. Cham: Springer International Publishing; 2020. p. 1-13.

34. Filidoro L, Dietrich O, Weber J, Rauch E, Oerther T, Wick M, et al. High-resolution diffusion tensor imaging of human patellar cartilage: Feasibility and preliminary findings. *Magnetic Resonance in Medicine*. 2005;**53**(5):993-8. doi: 10.1002/mrm.20469

35. Meder R, de Visser SK, Bowden JC, Bostrom T, Pope JM. Diffusion tensor imaging of articular cartilage as a measure of tissue microstructure. *Osteoarthritis and Cartilage*. 2006;**14**(9):875-81. doi: 10.1016/j.joca.2006.03.002

36. Raya JG, Melkus G, Adam-Neumair S, Dietrich O, Mützel E, Reiser MF, et al. Diffusion-tensor imaging of human articular cartilage specimens with early signs of cartilage damage. *Radiology*. 2013;**266**(3):831-41. doi: 10.1148/radiol.12120954

37. Schmitz N, Laverty S, Kraus VB, Aigner T. Basic methods in histopathology of joint tissues. *Osteoarthritis Cartilage*. 2010;**18 Suppl 3**:S113-6. doi: 10.1016/j.joca.2010.05.026

38. Petersen W, Tillmann B. Collagenous fibril texture of the human knee joint menisci. *Anatomy and Embryology*. 1998;**197**(4):317-24. doi: 10.1007/s004290050141

39. Norberg C, Filippone G, Andreopoulos F, Best TM, Baraga M, Jackson AR, et al. Viscoelastic and equilibrium shear properties of human meniscus: Relationships with tissue structure and composition. *Journal of Biomechanics*. 2021;**120**:110343. doi: doi.org/10.1016/j.jbiomech.2021.110343

40. Phelan N, Rowland P, Galvin R, O'Byrne JM. A systematic review and meta-analysis of the diagnostic accuracy of MRI for suspected ACL and meniscal tears of the knee. *Knee Surgery, Sports Traumatology, Arthroscopy*. 2016;**24**(5):1795. doi: doi.org/10.1007/s00167-015-3861-8

41. Falagas ME, Vardakas KZ, Vergidis PI. Under-diagnosis of common chronic diseases: prevalence and impact on human health. *International Journal of Clinical Practice*. 2007;**61**(9):1569-79. doi: 10.1111/j.1742-1241.2007.01423.x

42. Evers BJ, Schers HJ, van den Ende CHM, Thurlings RM, Koëter S. Diagnosing knee osteoarthritis in patients, differences between general practitioners and orthopedic surgeons: a retrospective cohort study. *BMC Primary Care*. 2023;**24**(1):155. doi: 10.1186/s12875-023-02107-4

43. Sjögren A, Bodahl S, Hughes V, Turkiewicz A, Aspberg A, Hellberg I, et al. Histological analysis of age-related degeneration in human female and male knee cartilage and meniscus. *Osteoarthritis and Cartilage Open*. 2026;**8**(1):100734. doi: 10.1016/j.ocarto.2025.100734

44. Pauli C, Grogan SP, Patil S, Otsuki S, Hasegawa A, Koziol J, et al. Macroscopic and histopathologic analysis of human knee menisci in aging and osteoarthritis. *Osteoarthritis and Cartilage*. 2011;**19**(9):1132-41. doi: 10.1016/j.joca.2011.05.008

45. Heijink A, Gomoll AH, Madry H, Drobnič M, Filardo G, Espregueira-Mendes J, et al. Biomechanical considerations in the pathogenesis of osteoarthritis of the knee. *Knee Surg Sports Traumatol Arthrosc*. 2012;**20**(3):423-35. doi: 10.1007/s00167-011-1818-0

46. Berberat JE, Nissi MJ, Jurvelin JS, Nieminen MT. Assessment of interstitial water content of articular cartilage with T1 relaxation. *Magnetic Resonance Imaging*. 2009;**27**(5):727-32. doi: 10.1016/j.mri.2008.09.005

47. Olsson E, Folkesson E, Peterson P, Önnerfjord P, Tjörnstrand J, Hughes HV, et al. Ultra-high field magnetic resonance imaging parameter mapping in the posterior horn of ex vivo human menisci. *Osteoarthritis and Cartilage*. 2019;**27**(3):476-83. doi: 10.1016/j.joca.2018.12.003

48. Pauwels E, Van Loo D, Cornillie P, Brabant L, Van Hoorebeke L. An exploratory study of contrast agents for soft tissue visualization by means of high resolution X-ray computed tomography imaging. *J Microsc*. 2013;**250**(1):21-31. doi: 10.1111/jmi.12013

49. Nieminen HJ, Gahunia HK, Pritzker KPH, Ylitalo T, Rieppo L, Karhula SS, et al. 3D histopathological grading of osteochondral tissue using contrast-enhanced micro-computed tomography. *Osteoarthritis and Cartilage*. 2017;**25**(10):1680-9. doi: 10.1016/j.joca.2017.05.021

50. Kestilä I, Thevenot J, Finnilä MA, Karhula SS, Hadjab I, Kauppinen S, et al. In vitro method for 3D morphometry of human articular cartilage chondrons based on micro-computed tomography. *Osteoarthritis and Cartilage*. 2018;**26**(8):1118-26. doi: 10.1016/j.joca.2018.05.012

51. van Geuns R-JM, Wielopolski PA, de Bruin HG, Rensing BJ, van Ooijen PMA, Hulshoff M, et al. Basic principles of magnetic resonance imaging. *Progress in Cardiovascular Diseases*. 1999;**42**(2):149-56. doi: 10.1016/S0033-0620(99)70014-9

52. Lehmann EH. Neutron Imaging Methods and Applications. In: Liang L, Rinaldi R, Schober H, editors. Neutron Applications in Earth, Energy and Environmental Sciences. Boston, MA: Springer US; 2009. p. 319-48.

53. Martell J, Alwmark C, Woracek R, Alwmark S, Hall S, Ferrière L, et al. Combined Neutron and X-Ray Tomography—A Versatile and Non-Destructive Tool in Planetary Geosciences. *Journal of Geophysical Research: Planets*. 2024;**129**. doi: 10.1029/2023JE008222

54. Behling R, Grüner F. Diagnostic X-ray sources—present and future. *Nuclear Instruments and Methods in Physics Research Section A: Accelerators, Spectrometers, Detectors and Associated Equipment*. 2018;**878**:50-7. doi: 10.1016/j.nima.2017.05.034

55. Bilderback DH, Elleaume P, Weckert E. Review of third and next generation synchrotron light sources. *Journal of Physics B: Atomic, Molecular and Optical Physics*. 2005;**38**(9):S773. doi: 10.1088/0953-4075/38/9/022

56. Streun A, Garvey T, Rivkin L, Schlott V, Schmidt T, Willmott P, et al. SLS-2 - the upgrade of the Swiss Light Source. *Journal of Synchrotron Radiation*. 2018;**25**(3):631-41. doi: 10.1107/S1600577518002722

57. Cramer KC. Lightening Europe: Establishing the European Synchrotron Radiation Facility (ESRF). *History and Technology*. 2017;**33**(4):396-427. doi: 10.1080/07341512.2018.1489762

58. Carpenter JM. The development of compact neutron sources. *Nature Reviews Physics*. 2019;**1**(3):177-9. doi: 10.1038/s42254-019-0024-8

59. Zakalek P, Gutberlet T, Brückel T. Neutron sources for large scale user facilities: The potential of high current accelerator-driven neutron sources. *Progress in Particle and Nuclear Physics*. 2025;**142**:104163. doi: 10.1016/j.ppnp.2025.104163

60. Sethi A. X-Rays: Interaction with Matter. Encyclopedia of Medical Devices and Instrumentation, Set.

61. Dewhurst C, Meyer A. Endurance – Modernisation of the instrumentation suite at the Institut Laue-Langevin. *EPJ Web Conf*. 2023;**286**:01001. doi: 10.1051/epjconf/202328601001

62. Bauer GS, Dai Y, Wagner W. SINQ layout, operation, applications and R&D to high power. *J Phys IV France*. 2002;**12**(8):3-26. doi: 10.1051/jp4:20020319

63. Nagamiya S. Introduction to J-PARC. *Progress of Theoretical and Experimental Physics*. 2012;**2012**(1). doi: 10.1093/ptep/pts025

64. Feldkamp LA, Davis LC, Kress JW. Practical cone-beam algorithm. *J Opt Soc Am A*. 1984;**1**(6):612-9. doi: 10.1364/JOSAA.1.000612

65. Strobl M, Manke I, Kardjilov N, Hilger A, Dawson M, Banhart J. Advances in neutron radiography and tomography. *Journal of Physics D: Applied Physics*. 2009;**42**(24):243001. doi: 10.1088/0022-3727/42/24/243001

66. Aregawi W, Defraeye T, Saneinejad S, Vontobel P, Lehmann E, Carmeliet J, et al. Dehydration of apple tissue: Intercomparison of neutron tomography with numerical modelling. *International Journal of Heat and Mass Transfer*. 2013;**67**:173-82. doi: 10.1016/j.ijheatmasstransfer.2013.08.017

67. Tudisco E, Etxegarai M, Hall SA, Charalampidou E-M, Couples GD, Lewis H, et al. Fast 4-D Imaging of Fluid Flow in Rock by High-Speed Neutron Tomography. *Journal of Geophysical Research: Solid Earth*. 2019;**124**(4):3557-69. doi: 10.1029/2018JB016522

68. Le Cann S, Tudisco E, Perdikouri C, Belfrage O, Kaestner A, Hall S, et al. Characterization of the bone-metal implant interface by Digital Volume Correlation of in-situ loading using neutron tomography. *Journal of the Mechanical Behavior of Biomedical Materials*. 2017;**75**:271-8. doi: 10.1016/j.jmbbm.2017.07.001

69. Isaksson H, Le Cann S, Perdikouri C, Turunen MJ, Kaestner A, Tägil M, et al. Neutron tomographic imaging of bone-implant interface: Comparison with X-ray tomography. *Bone*. 2017;**103**:295-301. doi: 10.1016/j.bone.2017.07.022

70. Törnquist E, Le Cann S, Tudisco E, Tengattini A, Andò E, Lenoir N, et al. Dual modality neutron and x-ray tomography for enhanced image analysis of the bone-metal interface. *Physics in Medicine & Biology*. 2021;**66**(13):135016. doi: 10.1088/1361-6560/ac02d4

71. Tengattini A, Lenoir N, Andò E, Giroud B, Atkins D, Beaucour J, et al. NeXT-Grenoble, the Neutron and X-ray tomograph in Grenoble. *Nuclear Instruments and Methods in*

Physics Research Section A: Accelerators, Spectrometers, Detectors and Associated Equipment. 2020;**968**:163939. doi: 10.1016/j.nima.2020.163939

72. Kaestner AP, Hartmann S, Kühne G, Frei G, Grünzweig C, Josic L, et al. The ICON beamline – A facility for cold neutron imaging at SINQ. *Nuclear Instruments and Methods in Physics Research Section A: Accelerators, Spectrometers, Detectors and Associated Equipment*. 2011;**659**(1):387-93. doi: 10.1016/j.nima.2011.08.022

73. Minniti T, Watanabe K, Burca G, Pooley DE, Kockelmann W. Characterization of the new neutron imaging and materials science facility IMAT. *Nuclear Instruments and Methods in Physics Research Section A: Accelerators, Spectrometers, Detectors and Associated Equipment*. 2018;**888**:184-95. doi: 10.1016/j.nima.2018.01.037

74. Bilheux HZ, Bilheux JC, Hanks RA, Byrd A, Jones A, Skorpenske H, et al. The VENUS imaging beamline at the Spallation Neutron Source: layout, expected performance and status of the construction project. *Journal of Physics: Conference Series*. 2023;**2605**(1):012004. doi: 10.1088/1742-6596/2605/1/012004

75. Shinohara T, Kai T, Oikawa K, Nakatani T, Segawa M, Hiroi K, et al. The energy-resolved neutron imaging system, RADEN. *Review of Scientific Instruments*. 2020;**91**(4):043302. doi: 10.1063/1.5136034

76. Birnbacher L, Braig E-M, Pfeiffer D, Pfeiffer F, Herzen J. Quantitative X-ray phase contrast computed tomography with grating interferometry. *European Journal of Nuclear Medicine and Molecular Imaging*. 2021;**48**(13):4171-88. doi: 10.1007/s00259-021-05259-6

77. Bravin A, Coan P, Suortti P. X-ray phase-contrast imaging: from pre-clinical applications towards clinics. *Physics in Medicine & Biology*. 2013;**58**(1):R1. doi: 10.1088/0031-9155/58/1/R1

78. Paganin D, Mayo SC, Gureyev TE, Miller PR, Wilkins SW. Simultaneous phase and amplitude extraction from a single defocused image of a homogeneous object. *Journal of Microscopy*. 2002;**206**(1):33-40. doi: 10.1046/j.1365-2818.2002.01010.x

79. Gureyev TE, Mayo SC, Myers DE, Nesterets Y, Paganin DM, Pogany A, et al. Refracting Röntgen's rays: Propagation-based x-ray phase contrast for biomedical imaging. *Journal of Applied Physics*. 2009;**105**(10). doi: 10.1063/1.3115402

80. Eckermann M, Töpperwien M, Robisch A-L, van der Meer F, Stadelmann C, Salditt T. Phase-contrast x-ray tomography of neuronal tissue at laboratory sources with submicron resolution. *Journal of Medical Imaging*. 2020;**7**(1):013502. doi: 10.1117/1.JMI.7.1.013502

81. Disney CM, Eckersley A, McConnell JC, Geng H, Bodey AJ, Hoyland JA, et al. Synchrotron tomography of intervertebral disc deformation quantified by digital volume correlation reveals microstructural influence on strain patterns. *Acta Biomaterialia*. 2019;**92**:290-304. doi: 10.1016/j.actbio.2019.05.021

82. Pierantoni M, Silva Barreto I, Hammerman M, Verhoeven L, Törnquist E, Novak V, et al. A quality optimization approach to image Achilles tendon microstructure by phase-contrast enhanced synchrotron micro-tomography. *Scientific Reports*. 2021;**11**(1):17313. doi: 10.1038/s41598-021-96589-w

83. Pierantoni M, Sharma K, Kok J, Novak V, Eliasson P, Isaksson H. Quantification of 3D microstructures in Achilles tendons during in situ loading reveals anisotropic fiber response. *Acta Biomaterialia*. 2025;**194**:246-57. doi: 10.1016/j.actbio.2025.01.023

84. Stampanoni M, Groso A, Isenegger A, Mikuljan G, Chen Q, Meister D, et al. TOMCAT: A beamline for TOmographic Microscopy and Coherent rAdiology experimenTs. *AIP Conference Proceedings*. 2007;**879**(1):848-51. doi: 10.1063/1.2436193

85. Rau C, Bodey A, Storm M, Cipiccia S, Marathe S, Zdora M-C, et al. Micro- and nano-tomography at the DIAMOND beamline I13L imaging and coherence: SPIE; 2017. doi: 10.1117/12.2274514

86. Cianciosi F, Buisson A-L, Tafforeau P, Van Vaerenbergh P. BM18, the new ESRF-EBS beamline for hierarchical phase-contrast tomography. *Proc 11th Mechanical Engineering Design of Synchrotron Radiation Equipment and Instrumentation*. 2021. doi: 10.18429/JACoW-MEDSI2020-MOIO02

87. Wilde F, Ogurreck M, Greving I, Hammel JU, Beckmann F, Hipp A, et al. Micro-CT at the imaging beamline P05 at PETRA III. *AIP Conference Proceedings*. 2016;**1741**(1):030035. doi: 10.1063/1.4952858

88. Gaj S, Yang M, Nakamura K, Li X. Automated cartilage and meniscus segmentation of knee MRI with conditional generative adversarial networks. *Magnetic Resonance in Medicine*. 2020;**84**(1):437-49. doi: 10.1002/mrm.28111

89. Lefevre N, Naouri JF, Herman S, Gerometta A, Klouche S, Bohu Y. A Current Review of the Meniscus Imaging: Proposition of a Useful Tool for Its Radiologic Analysis. *Radiology Research and Practice*. 2016;**2016**(1):8329296. doi: 10.1155/2016/8329296

90. Markhardt BK, Huang BK, Spiker AM, Chang EY. Interpretation of Cartilage Damage at Routine Clinical MRI: How to Match Arthroscopic Findings. *RadioGraphics*. 2022;**42**(5):1457-73. doi: 10.1148/rg.220051

91. Mayerhoefer ME, Welsch GH, Riegler G, Mamisch TC, Materka A, Weber M, et al. Feasibility of Texture Analysis for the Assessment of Biochemical Changes in Meniscal Tissue on T1 Maps Calculated From Delayed Gadolinium-Enhanced Magnetic Resonance Imaging of Cartilage Data: Comparison With Conventional Relaxation Time Measurements. *Investigative Radiology*. 2010;**45**(9):543-7. doi: 10.1097/RLI.0b013e3181ea363b

92. Bammer R. Basic principles of diffusion-weighted imaging. *European Journal of Radiology*. 2003;**45**(3):169-84. doi: 10.1016/S0720-048X(02)00303-0

93. Le Bihan D, Mangin JF, Poupon C, Clark CA, Pappata S, Molko N, et al. Diffusion tensor imaging: concepts and applications. *Journal of magnetic resonance imaging : JMRI*. 2001;**13**(4):534-46. doi: 10.1002/jmri.1076

94. O'Donnell LJ, Westin CF. An introduction to diffusion tensor image analysis. *Neurosurgery clinics of North America*. 2011;**22**(2):185-96, viii. doi: 10.1016/j.nec.2010.12.004

95. Duarte A, Ruiz A, Ferizi U, Bencardino J, Abramson SB, Samuels J, et al. Diffusion tensor imaging of articular cartilage using a navigated radial imaging spin-echo diffusion

(RAISED) sequence. *European radiology*. 2019;**29**(5):2598-607. doi: 10.1007/s00330-018-5780-9

96. Shen J, Zhao Q, Qi Y, Cofer G, Johnson GA, Wang N. Tractography of Porcine Meniscus Microstructure Using High-Resolution Diffusion Magnetic Resonance Imaging. *Frontiers in Endocrinology*. 2022;**Volume 13 - 2022**. doi: 10.3389/fendo.2022.876784

97. Van Nieuwenhove V, De Beenhouwer J, De Carlo F, Mancini L, Marone F, Sijbers J. Dynamic intensity normalization using eigen flat fields in X-ray imaging. *Opt Express*. 2015;**23**(21):27975-89. doi: 10.1364/OE.23.027975

98. Marone F, Stampanoni M. Regridding reconstruction algorithm for real-time tomographic imaging. *J Synchrotron Radiat*. 2012;**19**(Pt 6):1029-37. doi: 10.1107/s0909049512032864

99. Gursoy D, De Carlo F, Xiao X, Jacobsen C. TomoPy: a framework for the analysis of synchrotron tomographic data. *Journal of Synchrotron Radiation*. 2014;**21**(5):1188-93. doi: 10.1107/S1600577514013939

100. Kaestner AP. MuhRec—A new tomography reconstructor. *Nuclear Instruments and Methods in Physics Research Section A: Accelerators, Spectrometers, Detectors and Associated Equipment*. 2011;**651**(1):156-60. doi: 10.1016/j.nima.2011.01.129

101. Arnold O, Bilheux JC, Borreguero JM, Buts A, Campbell SI, Chapon L, et al. Mantid—Data analysis and visualization package for neutron scattering and μ SR experiments. *Nuclear Instruments and Methods in Physics Research Section A: Accelerators, Spectrometers, Detectors and Associated Equipment*. 2014;**764**:156-66. doi: 10.1016/j.nima.2014.07.029

102. Sjögren A, Bodahl S, Turkiewicz A, Ali N, Önnerfjord P, Englund M. 471 - Knee cartilage aging: histological analysis of donors without clinical knee disease aged 18 to 85 years. *Osteoarthritis and Cartilage*. 2025;**33**:S337. doi: 10.1016/j.joca.2025.02.477

103. Hennig J, Nauerth A, Friedburg H. RARE imaging: A fast imaging method for clinical MR. *Magnetic Resonance in Medicine*. 1986;**3**(6):823-33. doi: 10.1002/mrm.1910030602

104. Robson MD, Gatehouse PD, Bydder M, Bydder GM. Magnetic resonance: an introduction to ultrashort TE (UTE) imaging. *Journal of computer assisted tomography*. 2003;**27**(6):825-46. doi: 10.1097/00004728-200311000-00001

105. Schindelin J, Arganda-Carreras I, Frise E, Kaynig V, Longair M, Pietzsch T, et al. Fiji: an open-source platform for biological-image analysis. *Nature Methods*. 2012;**9**(7):676-82. doi: 10.1038/nmeth.2019

106. Dragonfly 2021.1 [Computer software]. Montreal, Canada: Comet Technologies Canada Inc.

107. Bankhead P, Loughrey MB, Fernández JA, Dombrowski Y, McArt DG, Dunne PD, et al. QuPath: Open source software for digital pathology image analysis. *Scientific Reports*. 2017;**7**(1):16878. doi: 10.1038/s41598-017-17204-5

108. Berg S, Kutra D, Kroeger T, Straehle CN, Kausler BX, Haubold C, et al. ilastik: interactive machine learning for (bio)image analysis. *Nature Methods*. 2019;**16**(12):1226-32. doi: 10.1038/s41592-019-0582-9

109. Sniekers YH, van Donkelaar CC. Determining Diffusion Coefficients in Inhomogeneous Tissues Using Fluorescence Recovery after Photobleaching. *Biophysical journal*. 2005;**89**(2):1302-7. doi: 10.1529/biophysj.104.053652

110. Kulmala KAM, Korhonen RK, Julkunen P, Jurvelin JS, Quinn TM, Kröger H, et al. Diffusion coefficients of articular cartilage for different CT and MRI contrast agents. *Medical Engineering & Physics*. 2010;**32**(8):878-82. doi: 10.1016/j.medengphy.2010.06.002

111. Singwi KS, Sjölander A. Diffusive Motions in Water and Cold Neutron Scattering. *Physical Review*. 1960;**119**(3):863-71. doi: 10.1103/PhysRev.119.863

112. Mills R. Self-diffusion in normal and heavy water in the range 1-45.deg. *The Journal of Physical Chemistry*. 1973;**77**(5):685-8. doi: 10.1021/j100624a025

113. Middendorf HD, Di Cola D, Cavatorta F, Deriu A, Carlile CJ. Water dynamics in charged and uncharged polysaccharide gels by quasi-elastic neutron scattering. *Biophysical Chemistry*. 1994;**53**(1):145-53. doi: 10.1016/0301-4622(94)00085-9

114. Chiapponi C, Di Bari MT, Gerelli Y, Deriu A, Chiessi E, Finelli I, et al. Water Dynamics in Physical Hydrogels Based On Partially Hydrophobized Hyaluronic Acid. *The Journal of Physical Chemistry B*. 2012;**116**(43):12915-21. doi: 10.1021/jp303657a

115. Mow VC, Guo XE. Mechano-Electrochemical Properties Of Articular Cartilage: Their Inhomogeneities and Anisotropies. *Annual Review of Biomedical Engineering*. 2002;**4**(1):175-209. doi: 10.1146/annurev.bioeng.4.110701.120309

116. Pavel Trtik MM, Timon Wehmann, Alessandro Tengattini, Duncan Atkins, E.H. Lehmann, Markus Strobl. PSI 'Neutron Microscope' at ILL-D50 Beamline – First Results. *Materials Research Proceedings*. 2020;**15**:23-8. doi: 10.21741/9781644900574-4

117. Andersen KH, Argyriou DN, Jackson AJ, Houston J, Henry PF, Deen PP, et al. The instrument suite of the European Spallation Source. *Nuclear Instruments and Methods in Physics Research Section A: Accelerators, Spectrometers, Detectors and Associated Equipment*. 2020;**957**:163402. doi: 10.1016/j.nima.2020.163402

118. Krug JR, van Schadewijk R, Vergeldt FJ, Webb AG, de Groot HJM, Alia A, et al. Assessing spatial resolution, acquisition time and signal-to-noise ratio for commercial microimaging systems at 14.1, 17.6 and 22.3 T. *Journal of Magnetic Resonance*. 2020;**316**:106770. doi: 10.1016/j.jmr.2020.106770

119. Saam T, Herzen J, Hetterich H, Fill S, Willner M, Stockmar M, et al. Translation of Atherosclerotic Plaque Phase-Contrast CT Imaging from Synchrotron Radiation to a Conventional Lab-Based X-Ray Source. *PLOS ONE*. 2013;**8**(9):e73513. doi: 10.1371/journal.pone.0073513

120. Morgan KS, Parsons D, Cmielewski P, McCarron A, Gradl R, Farrow N, et al. Methods for dynamic synchrotron X-ray respiratory imaging in live animals. *J Synchrotron Radiat*. 2020;**27**(Pt 1):164-75. doi: 10.1107/s1600577519014863

121. Hausermann D, Hall C, Maksimenko A, Campbell C. The Imaging and Medical Beam Line at the Australian Synchrotron. *AIP Conference Proceedings*. 2010;**1266**(1):3-9. doi: 10.1063/1.3478195

122. Karim A, Amin AK, Hall AC. The clustering and morphology of chondrocytes in normal and mildly degenerate human femoral head cartilage studied by confocal laser scanning microscopy. *Journal of Anatomy*. 2018;**232**(4):686-98. doi: 10.1111/joa.12768

123. Gratal P, Mediero A, Sánchez-Pernaute O, Prieto-Potin I, Lamuedra A, Herrero-Beaumont G, et al. Chondrocyte enlargement is a marker of osteoarthritis severity. *Osteoarthritis and Cartilage*. 2019;**27**(8):1229-34. doi: 10.1016/j.joca.2019.04.013

124. Hall AC. The Role of Chondrocyte Morphology and Volume in Controlling Phenotype—Implications for Osteoarthritis, Cartilage Repair, and Cartilage Engineering. *Current Rheumatology Reports*. 2019;**21**(8):38. doi: 10.1007/s11926-019-0837-6

125. Honkanen MKM, Saukko AEA, Turunen MJ, Shaikh R, Prakash M, Lovric G, et al. Synchrotron MicroCT Reveals the Potential of the Dual Contrast Technique for Quantitative Assessment of Human Articular Cartilage Composition. *Journal of orthopaedic research : official publication of the Orthopaedic Research Society*. 2020;**38**(3):563-73. doi: 10.1002/jor.24479

126. Silvast TS, Jurvelin JS, Lammi MJ, Töyräs J. pQCT study on diffusion and equilibrium distribution of iodinated anionic contrast agent in human articular cartilage – associations to matrix composition and integrity. *Osteoarthritis and Cartilage*. 2009;**17**(1):26-32. doi: 10.1016/j.joca.2008.05.012

127. Kokkonen HT, Mäkelä J, Kulmala KAM, Rieppo L, Jurvelin JS, Tiitu V, et al. Computed tomography detects changes in contrast agent diffusion after collagen cross-linking typical to natural aging of articular cartilage. *Osteoarthritis and Cartilage*. 2011;**19**(10):1190-8. doi: 10.1016/j.joca.2011.07.008

128. Fantoni S, Gabucci I, Cardarelli P, Paternò G, Taibi A, Cristofori V, et al. A Cationic Contrast Agent in X-ray Imaging of Articular Cartilage: Pre-Clinical Evaluation of Diffusion and Attenuation Properties. *Diagnostics*. 2022;**12**(9):2111. doi: 10.3390/diagnostics12092111

129. Walsh DA, Bonnet CS, Turner EL, Wilson D, Situ M, McWilliams DF. Angiogenesis in the synovium and at the osteochondral junction in osteoarthritis. *Osteoarthritis and Cartilage*. 2007;**15**(7):743-51. doi: 10.1016/j.joca.2007.01.020

130. Mapp PI, Walsh DA. Mechanisms and targets of angiogenesis and nerve growth in osteoarthritis. *Nature Reviews Rheumatology*. 2012;**8**(7):390-8. doi: 10.1038/nrrheum.2012.80

131. Han X, Maharjan S, Chen J, Zhao Y, Qi Y, White LE, et al. High-resolution diffusion magnetic resonance imaging and spatial-transcriptomic in developing mouse brain. *NeuroImage*. 2024;**297**:120734. doi: 10.1016/j.neuroimage.2024.120734

132. Jönsson V, Orozco GA, Pierantoni M, Dejea H, Gustafsson A, Grassi L, et al. Influence of articular cartilage sample geometry on mechanical response and properties using finite element simulation. *Journal of Biomechanics*. 2024;**176**:112323. doi: 10.1016/j.jbiomech.2024.112323

133. Donato S, Agostino RG, Arana Peña LM, Arfelli F, Brombal L, Longo R, et al. Unveiling tumor invasiveness: enhancing cancer diagnosis with phase-contrast microtomography for 3D virtual histology. *The European Physical Journal Plus*. 2024;**139**(5):413. doi: 10.1140/epjp/s13360-024-05188-x

134. Donato S, Arana Peña LM, Arfelli F, Brombal L, Colmo L, Longo R, et al. Integrating X-ray phase-contrast imaging and histology for comparative evaluation of breast tissue malignancies in virtual histology analysis. *Scientific Reports*. 2024;**14**(1):5831. doi: 10.1038/s41598-024-56341-6

135. Twengström W, Moro C, Romell J, Larsson J, Sparrelid E, Björnstedt M, et al. Can laboratory x-ray virtual histology provide intraoperative 3D tumor resection margin assessment? *Journal of Medical Imaging*. 2022;**9**(3):031503. doi: 10.1117/1.JMI.9.3.031503

136. Mow VC, Kuei SC, Lai WM, Armstrong CG. Biphasic Creep and Stress Relaxation of Articular Cartilage in Compression: Theory and Experiments. *Journal of Biomechanical Engineering*. 1980;**102**(1):73-84. doi: 10.1115/1.3138202

137. Eschweiler J, Horn N, Rath B, Betsch M, Baroncini A, Tingart M, et al. The Biomechanics of Cartilage—An Overview. *Life*. 2021;**11**(4):302. doi: 10.3390/life11040302

138. Basser PJ, Pierpaoli C. Microstructural and physiological features of tissues elucidated by quantitative-diffusion-tensor MRI. *Journal of Magnetic Resonance*. 2011;**213**(2):560-70. doi: 10.1016/j.jmr.2011.09.022